Title
MECHANICAL PROPERTIES OF LAVES PHASES

Author
Sasaki, Go.

Publication Date
1970-12-01

UCRL-20301

c.2

MECHANICAL PROPERTIES OF LAVES PHASES

Go Sasaki
(M. S. Thesis)

December 1970

AEC Contract No. W-7405-eng-48

LAWRENCE RADIATION LABORATORY
UNIVERSITY of CALIFORNIA BERKELEY

UCRL-20301
c.2

DISCLAIMER

TABLE OF CONTENTS

MECHANICAL PROPERTIES OF LAVES PHASES

Go Sasaki

Inorganic Materials Research Division, Lawrence Radiation Laboratory
Department of Materials Science and Engineering, College of Engineering
University of California, Berkeley, California

ABSTRACT

Primary interest in Laves phases in iron binary systems with transition elementslies in their effects as dispersed precipitates. The characteristics of Laves phases themselves should be made clear before discussing precipitation hardening. Mechanical properties of Laves phases, $NbFe_2$, $TaFe_2$, $TiFe_2$, $ZrFe_2$ and $HfFe_2$ have been studied by use of a micro Vickers hardness tester. The highest strength (over Hv. 1000) was obtained in $NbFe_2$ and $TaFe_2$, while the strength of $TiFe_2$ and $ZrFe_2$ was comparatively low (Hv. 859). The observation of the deformation around the hardness indentation showed that $TaFe_2$, $ZrFe_2$ and $HfFe_2$ seemed to deform partially with plastic form.

$NbFe_2$ and $TaFe_2$, which had almost the same strength but deformed differently were chosen for the study of their effects on the mechanical properties of the iron base binary alloys. Both higher strength and better ductility were obtained in the Fe-1.9 at.% Ta alloy than in Fe-1.78 at.% Nb alloy. A remarkable denuded zone at the retained δ grain boundaries was observed in the Fe-1.78 at.% Nb alloy.

I. INTRODUCTION

The Laves phase which was first established in the early 1930's by F. Laves is an intermediate compound with a stoichimetric composition of AB_2 in which the structure is primarily determined by the relative size of the atoms.

Most binary systems of iron with IVa, Va and VIa transition elements have Laves Phases, which appear as precipitates in useful alloys. In the iron base and nickel base super alloys for example Laves phases with various kinds of morphology always exist and are thought to increase the strength and decrease the ductility and the notch toughness at room temperature.[1] Laves phases are not confined to the transition metal systems. Many studies on the magnetic properties of Laves phases with non-transition elements have been done. Mainly due to their brittleness, however, only a few works[2-4] on the mechanical properties of Laves phases have been reported.

Here, the mechanical properties of the iron base Laves phases with IVa transition elements, i.e. Ti, Zr and Hf, and Va transition elements, i.e. Nb and Ta were studied by micro Vickers hardness tester. The observation of the deformation around the hardness indentation was carried out by using the interference-contrast method with reflected light and the scanning electron microscope.

G. R. Speich[5] investigated the precipitation behavior of Laves phases from iron-niobium and iron-titanium solid solution. Unfortunately, the mechanical properties of these alloys, however, were not reported, which makes quantitative analysis difficult due to the unknown relation between yield stress and hardness.

What kind of precipitate is desirable for designing alloys? Alloys containing strong particles incoherent with matrix can increase work-hardening rate because slip dislocations leaves loops around particles that they pass, and the effective interparticle spacing decreases as the number of loops increases. For coherent precipitates, slip dislocations must shear the particles in order to increase the yield stress.

Two high hardness Laves phases, $NbFe_2$ and $TaFe_2$ which showed different types of deformation in micro Vickers test, where chosen for the study of their effects on the mechanical properties of the iron base binary alloys. The effect of heat treatment on the morphology of precipitates was also investigated.

II. EXPERIMENTAL PROCEDURE

The experiment consists of two parts,(a) the mechanical properties of Laves phases, and (b) their effects as precipitates.

A. Material Preparation

The material used for the first part of the study was prepared from a button ingot (20.0 to 40.0 g) produced by an arc melting furnace (MRC Model AF-92C) and solution treated in quartz capsules evacuated and back filled with high purity argon. High purity raw materials were carefully selected for this study; 99.9% purity niobium and 99.9% tantalum powders were used as raw materials, and 99.9% purity sponges for titanium, zirconium and hafnium, and 99.999% purity powder for iron respectively. All alloys were turned and remelted from 3 to 6 times in order to prevent segregation. The ingots were invariably brittle. Some materials were shattered during cooling, which is due to the rapid cooling by the water cooled copper mold. Alloy No. 23 ($TaFe_2$) was remelted in the vacuum induction furnace in which the cooling velocity can be controlled to be relatively slow.

Table I shows the materials, melting method and the condition of the heat treatment.

The materials used for the second part of the study were prepared by vacuum induction melting of electrolytic iron (99.8%), high purity niobium rods (99.99%) and high purity tantalum (99.99%). The melts were vacuum cast as 1.00 to 1.25 in. diameter, 6 to 12 in. length ingots, which were hot rolled into a bar with 0.50 in. diameter in the temperature range 950 to 1000°C. Specimens of 0.50 in. diameter, 0.075 in. thickness were

TABLE I. Chemical composition, melting method and heat treatment of the Laves phases

No.	Composition (at.%)	Melting Method*	Solution Treatment
11	$NbFe_2$ (Nb 23.0)	AM (4)	1250°C, 24 hr.
12	$NbFe_2$ (Nb 33.0)	AM (3)	1300°C, 24 hr.
13	$NbFe_2$ (Nb 42.0)	AM (3)	1300°C, 24 hr.
21	$TaFe_2$ (Ta 27.0)	AM (4)	1350°C, 24 hr.
22	$TaFe_2$ (Ta 33.0)	AM (4)	1350°C, 24 hr.
23	$TaFe_2$ (Ta 33.0)	AM (5) - VIM (1)	1350°C, 24 hr.
31	$TiFe_2$ (Ti 25.0)	AM (4)	1250°C, 24 hr.
32	$TiFe_2$ (Ti 33.0)	AM (4)	1250°C, 24 hr.
33	$TiFe_2$ (Ti 35.0)	AM (5)	1250°C, 24 hr.
41	$ZrFe_2$ (Zr 23.0)	AM (4)	890°C, 7 days.
42	$ZrFe_2$ (Zr 33.0)	AM (6)	890°C, 7 days.
51	$HfFe_2$ (Hf 33.0)	AM (4)	1250°C, 24 hr.

*AM: Arc Melting, VIM: Vacuum Induction Melting. The number in parenthesis shows the times of remelting.

TABLE II. Chemical composition of the alloys

Alloy	At.% Nb	Wt.% Nb	At.% Ta	Wt.% Ta	Solution Treatment
Nb2	1.78	2.80	-	-	1380°C, 1 hr.
Ta2	-	-	1.96	6.04	1400°C, 1 hr.

cut from the rolled bar, sealed in quartz capsules evacuated and back filled with high purity argon gas, and heated in the δ phase region. The iron-niobium alloy and the iron-tantalum alloy were solution treated for 60 minutes at 1380°C and 1400°C, respectively, and quenched by smashing the capsules into 10% salt solution. In order to spheroidize the grain boundary precipitates, a transformation treatment i.e., α+Laves → γ+Laves → α+Laves, was carried out for 10 and 60 minutes at 1000°C, 1050°C and 1100°C, followed by air cooling. ASTM standard 0.25 in. round tension test specimens which were prepared by machining of the rolled bar were heat treated exactly in the same way.

The compositions of the alloy investigated were selected so that the alloys should have the same amount of precipitates at equilibrium condition. Alloy compositions and solution treatment are given in Table II.

B. X-Ray Analysis

Using Norelco type 12045 diffractometer with $CuK\alpha_1$ (λ:1.54050Å) radiation and monochromator, the crystal structure of Laves phases was checked. A powder of 100 mesh was prepared for the test. The diffraction patterns were determined by taking the average of at least two measured "d" (interplanar spacing) values. The analytical method[6] and Hull-Davey chart were used for indexing patterns of hexagonal, and cubic crystals respectively.

C. Optical Microscopy

Specimens prepared for microscopy were mechanically polished with emery papers and 1.0μ diamond paste, and then finished with 0.5μ Al_2O_3 particles. The echant used for No. 11 $NbFe_2$ (Nb 23.0 at.%), No. 21 $TaFe_2$

(Ta 27.0 at.%), No. 31 $TiFe_2$ (Ti 25.0 at.%) and No. 41 $ZrFe_2$ (Zr 23.0 at.%) was $FeCl_3$ solution and for other materials was Keller's concentrated eching solution and/or or 50% H_3PO_4 plus 50% HF solution.

The echant used for Nb2 and Ta2 was 2% and/or 5% Nital, depending on the condition of the heat treatment.

D. Micro Vickers Hardness Test

Hardness of Laves phases was measured at least ten times by using Leitz's MINILOAD hardness tester mostly with 300 gram load. A 100g load was used for No. 11 $NbFe_2$ (Nb 23.0 at.%), No. 21 $TaFe_2$ (Ta 27.0 at.%), and No. 41 $ZrFe_2$ (Zr 23.0 at.%). 1000 g and 2000 g loads were also used for the observation of the deformation around the hardness indentation.

Hardness of the aged specimens of Nb2 and Ta2 was determined from the average of five indentations made with 300 g load.

E. Interference-Contrast Method with Reflected Light

The interference-contrast method with reflected light(Zeiss' Ultraphot II) was employed for determining whether the deformation around the hardness indentation was due to slipping or cracking.

F. Scanning Electron Microscopy

Using JSM-U3 Scanning Electron Microscope (25 kV), the observation of the deformation around the indentation was carried out at higher magnifications (1,000X to 10,000).

This was widely used for the observation of the grain boundaries and the morphology of the precipitates in Nb2 and Ta2. The fracture surface of tensile specimen was also observed by the scanning electron microscope.

G. Tensile Test

An Instron (TT-Model, Instron Eng. Coop) was used for the tensile testing of Nb2 and Ta2. A cross head speed of 0.1 cm per second was employed. The tensile test specimens were ASTM standard 0.25 in. round bar type with 1.000 in. gage length. The yield stress was determined by taking the 0.2% offset strain.

III. RESULTS AND DISCUSSION

A. Mechanical Properties of Laves Phases

1. Phase Diagram

Figures 1 to 5 show the latest equilibrium phase diagrams[7-9] of the systems, on which the compositions used for this study are marked. The theoretical range of Laves phase based on the high temperature phase diagram proposed by L. Brewer[10] is also shown. In the iron binary system with IVa, Va and VIa elements, there exist Laves phases, $TiFe_2$, $ZrFe_2$, $HfFe_2$, $NbFe_2$, $TaFe_2$ and WFe_2. The compound $MoFe_2$ has not been decisively confirmed. Pure WFe_2 is hard to obtain because of the many intermetallic compounds in the system. Several attempts to make a pure WFe_2 had been done by the author, however, several other phases were formed which could not be eliminated even with a long time heat treatment.

Five systems were chosen for this study. As shown in Figs. 1 to 5 $TiFe_2$, $HfFe_2$ and $NbFe_2$ have large solubility ranges, and $ZrFe_2$ and $TaFe_2$ have pin-point solubility. Brewer[10] proposed a large solubility ranges for $ZrFe_2$(Zr 28 to 37 at.%) and $TaFe_2$ (Ta 26 to 35 at.%).

Figures 6 to 10 show the microstructures of the material used for this study. Specimens No. 11 (Nb 23.0 at.%), No. 21 (Ta 27.0 at.%), No. 31 (Ti 25.0 at.%) and No. 41 (Zr 23.0 at.%) consisted of two phases (α-Fe and Laves phase) as shown clearly in the microstructures. The difference of microstructures between No. 22 and No. 23 which contain the same amount of tantalum is considered to be due to the difference of the melting process. Number 42 (Zr 33.0 at.%) seems to have two different phases. However, it is likely to be a purer Laves phase since the

X-ray diffraction pattern does not show any distinct evidence of the existence of another phase. Specimens No. 12 (Nb 33.0 at.%), No. 13 (Nb 42.0 at.%), No. 22 and 23 (both Ta 33.0 at.%), No. 32 (Ti 33.0 at.%), No. 33 (Ti 35.0 at.%) and No. 51 (Hf 33.0 at.%) are considered to be pure Laves phases.

The hardness measurement of the material is given in Table III, and also graphed in Fig. 11. Yields between before and after casting were almost 100%. Figure 1 shows that the $NbFe_2$ Laves phase has a solubility extending from 23.0 to 42.0 at.%. The present work indicates that the minimum solubility of niobium in $NbFe_2$ may be larger than 23.0 at.%. For Fig. 6 (a) shows the existence of a fairly large amount of α-Fe. Similarly, as shown in Fig. 3 the $TiFe_2$ Laves phase has a solubility of 25.0 to 35.0 at.%. This work indicates that the iron-rich side of $TiFe_2$ is actually larger than 25.0 at.%, which is clearly shown by the microstructure (Fig. 8(a)).

2. Crystal Structure

The Laves phase are characterized by three crystal structures, i.e. $MgCu_2$, cubic C15 type (Fig. 12), $MgZn_2$, hexagonal C14 type (Fig. 13a, b) and $MgNi_2$, hexagonal C36 type (Fig. 13c).

As shown in Fig. 12b, Fig. 13a and 13b, the $MgCu_2$ structure consists of the atomic layers stacked PQRPQR, while $MgZn_2$ consists of those PQPQPQ. $MgNi_2$ may be regarded as a transition phase between $MgCu_2$ and $MgZn_2$ with a stacking of PQPRPQPR.

The crystal structure, the electron per atom ratio and the lattice parameter of the material for this study are given in Table IV. $NbFe_2$, $TaFe_2$ and $TiFe_2$ have the hexagonal $MgZn_2$ type structure, while $ZrFe_2$ has

the cubic $MgCu_2$ type. The crystal structure of $HfFe_2$ has not been determined as yet. Hansen et al[7] and W. B. Pearson[11] reported that $HfFe_2$ exhibited a duplex structure of $MgZn_2$ with $MgCu_2$. On the other hand, R. P. Elliott[12] reported that $HfFe_2$ showed a diffraction pattern isomorphous with the $MgNi_2$ structure.

The X-ray diffraction patterns of each Laves phase are shown in Figs. 14 to 18. $NbFe_2$, $TaFe_2$, $TiFe_2$ and $HfFe_2$ were confirmed to have a hexagonal unit cell structure and $ZrFe_2$ was cubic. A slight difference of "d" (interplanar spacing) values in $NbFe_2$ (Fig. 14) and $TiFe_2$ (Fig. 16) between the present work and ASTM data is probably due to the difference of niobium and tantalum contents between the two works, i.e. the difference of lattice parameters. ASTM data originally given by Speich[5] is on the precipitates extracted from Fe-1.67 wt.% Nb and Fe-5.8 wt.% Ti alloys, i.e., the iron-rich sides of Laves phases. The diffraction patterns of $ZrFe_2$ (Fig. 17) agreed with that of ASTM. Though crystallographic data for $TaFe_2$ has not been described in the ASTM card files, the present work (Fig. 15) shows that it has a hexagonal structure, the interplanar spacing values of which are similar to that of $TiFe_2$. Figure 18 suggests that $HfFe_2$ has a $MgZn_2$ type structure.

R. P. Elliott and W. Rostoker,[14] A. G. Dwight,[15] and V. M. Nevitt[16] have discussed in detail the various factors which determine the occurrence of Laves phase. It is now quite evident that the atomic size and the electron per atom ratio are two major factors for the occurrence of the phase. A. G. Dwight[15] showed that Laves phases form in the range of Goldschmidt radius ratios from 1.06 to 1.65 for the cubic $MgCu_2$ type structure, 1.05 to 1.40 for the hexagonal $MgZn_2$ and the hexagonal $MgNi_2$

type structures, and reported that the major factor controlling the formation of Laves phases is the ability of the partner elements to contract or expand so that the ideal ratio 1.225 is approached. As shown in Table IV, the Goldschmidt radius ratios of the Laves phases obtained in this study satisfy his criterion.

For the second factor, Decker et al[1] reported that there exists a distinct boundary of electron per atom ratio under 8.0 for the appearance of Laves phase.

3. Hardness

The measured hardness is given in Table III, and graphed in Fig. 11. As shown in Fig. 11, the hardness of $NbFe_2$ was the highest in all the materials (Hv. 1063). $TaFe_2$ also showed high hardness (Hv. 1010). The hardness of $TiFe_2$ and $ZrFe_2$, on the other hand, was relatively low (Hv. 859 for both). $HfFe_2$ showed Hv. 943. In the Laves phases with IVa element, the greater the atomic number of transition element, the higher the hardness. The hardness of Va group was much higher than that of IVa group.

4. Observation of the Deformation around the Hardness Indentation

The observation of the deformation around the micro Vickers hardness indentation was carried out by using both the interference-contrast technique with reflected light and the scanning electron microscope. Figures 19 to 23 and Figs. 24 to 32 show typical examples to illustrate the deformation around the hardness indentation observed by the interference-contrast method and the scanning electron microscope, respectively.

As shown in the photographs, clear-cut slip bands or slip lines could not be observed around the hardness indentation of all specimens. It is, however, evident that the types of deformation between $NbFe_2$ and $TaFe_2$, for example, are quite different. It can be said that relative ductility can be evaluated qualitatively from the shape and the length of the deformation. If there is no plastic deformation, the hardness cannot be measured.

The work done by the hardness testing, W, consists of the three terms, i.e., the work compensated in making indentation, w_1, the work compensated in other things raising the heat, for example, w_3, which can be negligible in this case. When the hardness of two specimens are almost the same, then these w_2 terms should not be different because W, w_1 and w_3 are the same. The term w_2 can be expressed by the energy terms, i.e., the energy for crack nucleation, E_1 and the energy for a crack propagation, E_2. E_2 consists of the work in making free surface w_4, and the work spent in plastic deformation, w_5. If E_1 does not change much in two specimens, the one with short cracks has greater w_5, and is actually less brittle than the one with longer cracks.

First, the cracks observed in $NbFe_2$ started at four corners which have highest stress concentration, and propagated straightly to a length of approximately 90μ. We shall call this type of deformation "A".

Second, the cracks of $TaFe_2$, the hardness of which was nearly the same as that of $NbFe_2$, started mainly at the corners, but their shapes became wavy and their length relatively short (average 38.8μ). We shall call this type "B". And as shown in Figs. 20 and 26, some regions which seemed to deform plastically were observed. We shall call this type "C". $TaFe_2$

could be more ductile at room temperature than $NbFe_2$ because of the shorter crack length.

Third, the cracks in $TiFe_2$ started not only at the corners but the edges, and became wavier, (type B). Its crack length was 41μ. The types of deformation observed in $ZrFe_2$ and $HfFe_2$ were quite similar. Both had about the same crack length, 62μ for $ZrFe_2$ and 60μ for $HfFe_2$, (type A) and also type C deformation.

The summary of those observation is given in Table V.

No reports on the plastic deformation of Laves phase at room temperature have been made except a short note on $HoZn_2$.[3] D. J. Michel and E. Ryba conducted compression tests on $HoZn_2$ at room temperature and showed that the specimen after testing revealed considerable cross-twinning as well as additional other type twins. This was concluded as a direct evidence for a small amount of localized plastic deformation. The same authors reported in recent work[4] that there was no detectable plastic deformation since a plot of stress against the average strain above the low stress-low strain region was found to be linear. D. J. Moran[2] found that the compressive ductility of a single crystal of $MgCu_2$ began at 450°C ($0.65T/T_m$). The tensile ductility was characterized by an abrupt brittle-ductile transition at 600°C ($0.8\ T/T_m$).

B. The Effects of Precipitation of $NbFe_2$ and $TaFe_2$ on the Mechanical Properties of Fe-1.78 at.% Nb and Fe-1.96 at.% Ta Alloys

Two high hardness Laves phases, $NbFe_2$ which deformed (type A) and $TaFe_2$ (types B and C) were chosen. The iron-rich side of those phase diagrams is shown in Fig. 33. No other precipitates except Laves phases $NbFe_2$ for Nb2 and $TaFe_2$ for Ta2, form in these systems.

1. Aging Kinetics

The structures of Nb2, i.e., Fe-1.78 at.% Nb alloy and Ta2, i.e., Fe-1.96 at.% Ta alloy when quenched from δ phase region consisted of homogeneous ferrite with a grain size of about ASTM No. 1 (Fig. 34).

As shown in Figs. 35 and 36, the precipitation-hardening behavior of Nb2 and Ta2 are quite similar except that the hardness peaks of Nb2 are shifted to a shorter time. Aging at 600°C, 700°C, and 800°C in both alloys showed single peaks. Figure 37 shows the microstructures of these alloys which correspond to the aging peak at 700°C.

Speich[5] who worked on Fe-3.80 wt.% Nb alloy, reported that precipitation occurs first at grain boundary, then dislocations and finally in the matrix. The precipitates were found to be plate-like and formed on $\{110\}_\alpha$.

2. Mechanical Properties of Fe-1.78 at.% Nb and Fe-1.96 at.% Ta Alloys

As shown in Fig. 37, both alloys have massive continuous precipitates at grain boundary, which are detrimental to the ductility of the material. In order to make the massive grain boundary precipitates discontinuous and spheroidized, the transformation treatment suggested by R. H. Jones[17] was employed. Materials were heated in the γ+Laves phase region, i.e. at temperatures of 1100°C, 1050°C and 1000°C, and held for 10 and 60 minutes, followed by air cooling.

The mechanical properties of these materials are given in Table VI. Ta2 specimens displayed higher strength and better ductility than Nb2. The longer the transformation treatment and the higher the temperature of the transformation treatment, the better the ductility of the specimens. This tendency is evident in Ta2.

Figures 38 and 39 show the optical microstructures of Nb2 and Ta2, which were air cooled from 1100°C and 1000°C. Here, the matrix transforms twice, i.e. the ferrite with bcc structure first changes to austenite (with fcc structure), which transforms again to ferrite (with bcc structure) by slow cooling from the austenite region.

The morphology of the precipitates is shown more clearly in the scanning electron microstructure; Fig. 40 for Nb2 and Fig. 41 for Ta2. The grain boundary precipitate of 1100°C for 60 minutes treatment was almost completely spheroidized, while that of 1000°C treatment was only partially spheroidized. That of 1050°C was the intermediate stage between these two. Coarsening of the precipitates was more dominant in Nb2 than Ta2.

There are no diffusion data available for niobium and tantalum in iron, but it is considered that their activation parameters including the diffusion coefficient would not differ much due to the small difference of atomic radius between the two elements. Furthermore, as shown in Fig. 40 a large number of needle-like precipitates which are considered to be unstable, were observed in the Nb2 specimen of 1000°C, 60 min. transformation treatment. It turns out that drastic change of morphology of the precipitate in Nb2 would not be explained simply by the diffusion theory. The difference of the matrix-precipitate interface reaction and the surface energy of the precipitates between the two alloys is thought to play an important role in the transformation treatment.

Jones et al.[18] reported the existence of a precipitate-free zone lying adjacent to the grain boundary and adjacent to clusters of dislocation-nucleated precipitate in aged Fe-1.8 wt.% Nb alloy. As shown in Figs. 40

and 41, the denuded zone at the retained δ grain boundary is predominant in Nb2. Figure 42 shows the niobium change across a retained δ grain boundary which was analyzed continuously with 0.5μ steps by an electron microprobe analyzer (MAC's Model 400). In case of Ta2, the tantalum change could not be observed because of the narrow depleted zone.

Figure 43 shows the scanning electron mircographs of the fractured surface. The fracture of Nb2 occurred at the retained δ grain boundary.

Figure 43(b) shows a lot of dimples in the Ta matrix. Tensile specimens of Nb2 fractured intergranularly at the retained δ grain boundary is the main cause of low strength and low ductility. Those of Ta2, on the other hand, fractured transgranularly (at the δ grain boundary), resulted in higher elongation and higher reduction of area.

SUMMARY AND CONCLUSIONS

The mechanical properties of the Laves phase, $NbFe_2$, $TaFe_2$, $TiFe_2$, $ZrFe_2$ and $HfFe_2$ have been studied by using a micro Vickers hardness tester.

1. The highest strengths, over Hv. 1000, was obtained in $NbFe_2$ and $TaFe_2$. The hardness of $TiFe_2$ and $ZrFe_2$ was relatively low (Hv. 859). $HfFe_2$ showed intermediate hardness (Hv. 943).

2. From the observation of the deformation around the hardness indentation, $TaFe_2$ is considered to be more ductile than $NbFe_2$. $NbFe_2$ deformed in more brittle way, while $TaFe_2$, $ZrFe_2$ and $HfFe_2$ appeared to deform plastically.

The effects of $NbFe_2$ and $TaFe_2$ on the mechanical properties of the Fe-1.78 at.% Nb and Fe-1.96 at.% Ta alloys have been investigated.

3. By a transformation treatment, continuous grain boundary precipitates can be spheroidized.

4. Both the strength and ductility of the Fe-1.96 at.% Ta alloy were superior to those of the Fe-1.78 at.% Nb alloy. The former fractured transgranularly at the retained δ grain boundaries and the latter fractured intergranularly.

5. A remarkable grain boundary denuded zone was observed in the Fe-1.78 at.% Nb alloy, while not in the Fe-1.96 at.% Ta alloy.

6. For future work, an investigation of the thermo-mechanical treatment a and the heat treatment of binary and ternary alloys might be studied in order to improve the mechanical properties. The high temperatures properties (creep rupture, oxidation, etc.) as well as the room temperature properties in ternary or quartinary systems would be of interest.

ACKNOWLEDGEMENTS

The author wishes to express his appreciation and deep gratitude to Professor Victor F. Zackay and Professor Earl R. Parker for their continued guidance, support and encouragements throughout the course of this investigation. Special thanks are due to Mr. George Golden and Mr. Russel H. Johns for the helpful suggestions and discussions.

Thanks are also due to Mrs. Gloria Pelatowski for her help in preparing the art work and to Mrs. Shirley Ashley, Miss Jane Ball and Mrs. Linda LeBorgne for their help in typing.

This work was performed under the auspices of the U.S. Atomic Energy Commission through the Inorganic Materials Research Division of the Lawrence Radiation Laboratory, Berkeley.

TABLE III. Structure and hardness of the Laves phase

No.	Compositions (at.%)	Structure	Range	Hardness (Hv) Average
11	Nb 23.0	α-Fe	308-390	349.0
		$NbFe_2$	582-762	672.0
12	Nb 33.0	$NbFe_2$	1051-1097	1076.3
13	Nb 42.0	$NbFe_2$	1028-1097	1049.0
21	Ta 27.0	α-Fe	322-472	397.0
		$TaFe_2$	685-762	736.3
22	Ta 33.0	$TaFe_2$	954-1019	983.3
23	Ta 33.0	$TaFe_2$	998-1089	1035.7
31	Ti 25.0	α-Fe	346-501	424.0
		$TiFe_2$	730-810	770.7
32	Ti 33.0	$TiFe_2$	792-845	821.2
33	Ti 35.0	$TiFe_2$	845-923	886.4
41	Zr 23.0	α-Fe (entectic)	420-493	461.1
		$ZrFe_2$	864-940	914.2
42	Zr 33.0	$ZrFe_2$	826-894	859.3
51	Hf 33.0	$HfFe_2$	898-982	942.9

TABLE IV. Crystal structure, electron-atom ratio and lattice parameter of the Laves phases.

Laves Phase	Crystal Structure	Electron: Atom Ratio	Lattice Parameter*1 (Å) C	(Å) A	C/A	Goldschmidt Radius Ratio*2
$NbFe_2$	$MgZn_2$	7.00	7.880	4.834	1.630	1.137
$TaFe_2$	$MgZn_2$	7.00	7.838	4.827	1.624	1.138
$TiFe_2$	$MgZn_2$	6.67	7.761	4.799	1.624	1.137
$ZrFe_2$	$MgCu_2$	6.67	-	7.053	-	1.250
	$MgCu_2$*3	6.67	-	7.025	-	
$HfFe_2$	$MgZn_2$	6.67	8.124	4.978	1.631*4	1.236
	$MgNi_2$	6.67	16.167	4.968	3.254*5	

*1 From "Handbook of Lattice Spacing and Structure of Metals and Alloys"[11]

*2 From (7). Radii of Zr and Hf are from (13)

*3 Allotropic modification occuring at low temperature

*4 From (7)

*5 From (12)

TABLE V. Observation of deformation around the hardness indentations

Laves Phase	Observation of Deformation	Crack length at the corner (μ)	Type of Deformation
$NbFe_2$	Long straight cracks at the corners	159.6-66.4 av. 91.2	A
$TaFe_2$	Short wavy cracks mainly at the corners	30.2-47.3 av. 38.8	B and C
$TiFe_2$	Short wavy cracks at the corners and the edges	37.5-50.0 av. 40.8	B
$ZrFe_2$	Long straight cracks at the corners Plastically deformed region	57.3-74.5 av. 62.2	A and C
$HfFe_2$	Long straight cracks at the corners Plastically deformed region	44.3-77.6 av. 60.2	A and C

Type A refers to specimens with long straight cracks at the corners

Type B refers to specimens with wavy short cracks both at the corners and edges.

Type C refers to specimens which appear to deform plastically.

TABLE VI. Tensile properties of the alloys

Material	Heat Treatment (°C, min.)	Yield Stress 0.2% psi	Tensile Strength psi	Elongation %	Reduction of area %
Nb2	1380, 60WQ 700, 30AC 1100, 10AC	49,400	58,800	3.2	8.8
Nb2	1380, 60WQ 700, 30AC 1100, 60AC	51,700	58,300	5.1	33.9
Nb2	1380, 60WQ 700, 30AC 1050, 60AC	47,700	61,900	7.4	20.6
Nb2	1380, 60WQ 700, 30AC 1000, 60AC	42,200	47,200	3.2	11.5
Ta2	1400, 60WQ 700, 40AC 1100, 10AC	50,200	69,600	18.9	33.9
Ta2	1400, 60WQ 700, 40AC 1100, 60AC	48,600	68,200	31.1	68.8

REFERENCES

1. R. E. Decker and S. Floreen, Copyright AIMR, p. 69, (1965).
2. J. B. Moran, Trans. of Met. Society of AIMR, Vol. 233, p. 1473 (1965).
3. D. J. Michel and E. Ryba, Trans. of Met. Society of AIME,Vol. 235, p.436, (1969).
4. D. J. Michel and E. Ryba, Met. Trans, Vol. 1, p. 544 (1970).
5. G. R. Speich, Trans. of Met. Society of AIME, Vol. 224, p. 850 (1962).
6. T. B. Massalski and H. E. King, Tables of Crystallographic Functions for Calculating Lattice Parameters of hcp Metals and Alloys from X-ray Diffraction Data, Mellon Institute (1960).
7. M. Hansen, and K. Anderko, Constitution of Binary Alloys, McGraw-Hill, New York (1958).
8. R. P. Elliott, ibid. Suppl. (1965).
9. F. A. Shunk, ibid. Suppl. (1969).
10. L. Brewer, Prediction of High Temperature Metallic Phase Diagrams, UCRL-10701, (1965).
11. W. B. Pearson, Handbook of Lattice Spacings and Structures of Metals and Alloys, Pergamon Press, New York (1958).
12. R. P. Elliott, Trans. of ASM, Vol. 53, p. 321 (1961).
13. E. D. Gibson, B. A. Loomis and O. H. Carlson, Trans. of ASM, Vol. 50, p. 178 (1953).
14. R. P. Wlliott and E. Rostoker, Trans. of ASM, Vol. 50, p. 617 (1958).
15. A. E. Dweight, Trans. of ASM, Vol. 53, p. 476 (1961).
16. V. M. Nevitt, "Alloy Chemistry of Transition Elements", paper in Electronic Structure and Alloy Chemistry of the Transition Elements, P. A. Beck, Ed., Interscience Publ., New York, 1963.

17. R. H. Jones, to be published.

18. R. M. F. Jones and D. R. F. West, Journal of the Iron and Steel Institute, p. 270 (March 1970).

FIGURE CAPTIONS

Fig. 1. Equilibrium phase diagram: Fe-Nb system.[8]

Fig. 2. Equilibrium phase diagram: Fe-Ta system.[7]

Fig. 3. Equilibrium phase diagram: Fe-Ti system.[8]

Fig. 4. Equilibrium phase diagram: Fe-Zr system.[7]

Fig. 5. Equilibrium phase diagram: Fe-Hf system.[9]

Fig. 6. Micrograph: (a) Nb 23.0 at.%, (b) Nb 33.0 at. %, (c) Nb 42.0 at.%, 150×

Fig. 7. Micrograph: (a) Ta 27.0 at.%, (b) Ta 33.0 at. %, (c) Ta 33.0 at. %, 150×

Fig. 8. Micrograph: (a) Ti 25.0 at. %, (b) Ti 33.0 at. %, (c) Ti 35.0 at. %, 150×

Fig. 9. Micrograph: (a) Zr 23.0 at. %, (b) Zr 33.0 at. %, 150×

Fig. 10. Micrograph: Hf 33.0 at. %, 150×

Fig. 11. Micro Vickers hardenss of Laves phases.

Fig. 12. (a) Crystal structures of $MgCu_2$
(b) Rows of Mg atoms

Fig. 13. (a) Crystal structure of $MgZn_2$
(b) Rows of Mg atoms in $MgZn_2$
(c) Rows of Mg atoms in $MgNi_2$

Fig. 14. X-ray diffraction data for $NbFe_2$.

Fig. 15. X-ray diffraction data for $TaFe_2$.

Fig. 16. X-ray diffraction data for $TiFe_2$.

Fig. 17. X-ray diffraction data for $ZrFe_2$.

Fig. 18. X-ray diffraction data for $HfFe_2$.

Fig. 19. Interference micrograph of the hardenss indentation: $NbFe_2$ (Nb 33.0 at. %), 300 g load, 1000×.

Fig. 20. Interference micrograph of the hardenss indentation:
(a) $TaFe_2$ (Ta 27.0 at. %), 100 g load, 800×
(b) $TaFe_2$ (Ta 33.0 at. %), 2000 g load, 800×

Fig. 21. Interference micrograph of the hardness indentation:
$TiFe_2$ (Ti 35.0 at. %), 300 g load, 800×

Fig. 22. Interference micrograph of the hardness indentation:
$ZrFe_2$ (Zr 33.0 at. %), 300 g load, 800×

Fig. 23. Interference micrograph of the hardness indentation:
$HfFe_2$ (Hf 33.0 at. %), 300 g load, 800×

Fig. 24. Scanning electron micrograph of the hardness indentation:
(a) $NbFe_2$ (Nb 33.0 at. %), 300 g load, 2000×,
(b) higher magnification of (a), 4000×

Fig. 25. Scanning electron micrograph of the hardness indentation:
(a) $NbFe_2$ (Nb 42.0 at. %), 500 g load, 1000×
(b) higher magnification of (a), 5000×

Fig. 26. Scanning electron micrograph of the hardness indentation:
(a) $TaFe_2$ (Ta 33.0 at. %), 300 g load, 2000×
(b) higher magnification of (a), 5000×

Fig. 27. Scanning electron micrograph of the hardness indentation:
(a) $TaFe_2$ (Ta 33.0 at. %), 300 g load, 2000×
(b) $TaFe_2$ (Ta 33.0 at. %), 300 g load, 2000×

Fig. 28. Scanning electron micrograph of the hardness indentation:
(a) $TiFe_2$ (Ti 25.0 at. %), 300 g load, 2000×
(b) higher magnification of (a), 10,000×

Fig. 29. Scanning electron micrograph of the hardness indentation:
(a) $TiFe_2$ (Ti 33.0 at. %), 300 g load, 2000×
(b) higher magnification of (a), 4000×

Fig. 30. Scanning electron micrograph of the hardness indentation:
(a) $TiFe_2$ (Ti 35.0 at. %), 300 g load, 2000×
(b) $TiFe_2$ (Ti 35.0 at. %), 300 g load, 2000×

Fig. 31. Scanning electron micrograph of the hardness indentation:
(a) $ZrFe_2$ (Zr 33.0 at. %), 300 g load, 2000×
(b) $ZrFe_2$ (Zr 33.0 at. %), 300 g load, 2000×

Fig. 32. Scanning electron micrograph of the hardness indentation:
(a) $HfFe_2$ (Hf 33.0 at. %), 300 g load, 2000×
(b) $HfFe_2$ (Hf 33.0 at. %), 300 g load, 2000×

Fig. 33. Phase diagrams (iron-rich sides) of Fe-Nb and Fe-Ta systems.

Fig. 34. Micrograph: (a) Nb_2, solution treated, 200×
(b) Ta_2, solution treated, 200×

Fig. 35. Aging kinetics of Nb_2.

Fig. 36. Aging kinetics of Ta_2.

Fig. 37. Scanning electron micrograph: (a) Nb_2, 700°C for 30 min., 10,000×, (b) Ta_2, 700°C for 40 min., 10,000×

Fig. 38. Micrograph: (a) Nb_2, 700°C for 30 min. and 1100°C for 60 min. AC, 2000×, (b) Nb_2, 700°C for 30 min. AC and 1000°C for 10 min. AC, 2000×

Fig. 39. Micrograph: (a) Ta_2, 700°C for 40 min. AC and 1100°C for 60 min. AC, 2000× (b) Ta_2, 700°C for 40 min. AC and 1000°C for 10 min. AC, 2000×

Fig. 40. Scanning electron micrograph of Nb_2:
(a) 700°C for 30 min. AC and 1100°C for 60 min. AC, 7000×
(b) 700°C for 30 min. AC and 1050°C for 60 min. AC, 7000×
(c) 700°C for 30 min. AC and 1000°C for 60 min. AC, 7000×

Fig. 41. Scanning electron micrograph of Nb_2:
(a) 700°C for 40 min. AC and 1100°C for 60 min. AC, 7000×,
(b) 700°C for 40 min. AC and 1050°C for 60 min. AC, 7000×
(c) 700°C for 40 min. AC and 1000°C for 60 min. AC, 7000×

Fig. 42. Niobium change at the grain boundary of Nb_2 (microprobe analyzer).

Fig.43. Scanning electron micrographs of the fractured surface:
(a) Nb_2, 700°C for 30 min. AC and 1100°C for 60 min. AC, 100×, (b) Ta_2, 700°C for 40 min. AC and 1100°C for 60 min. AC, 100×.

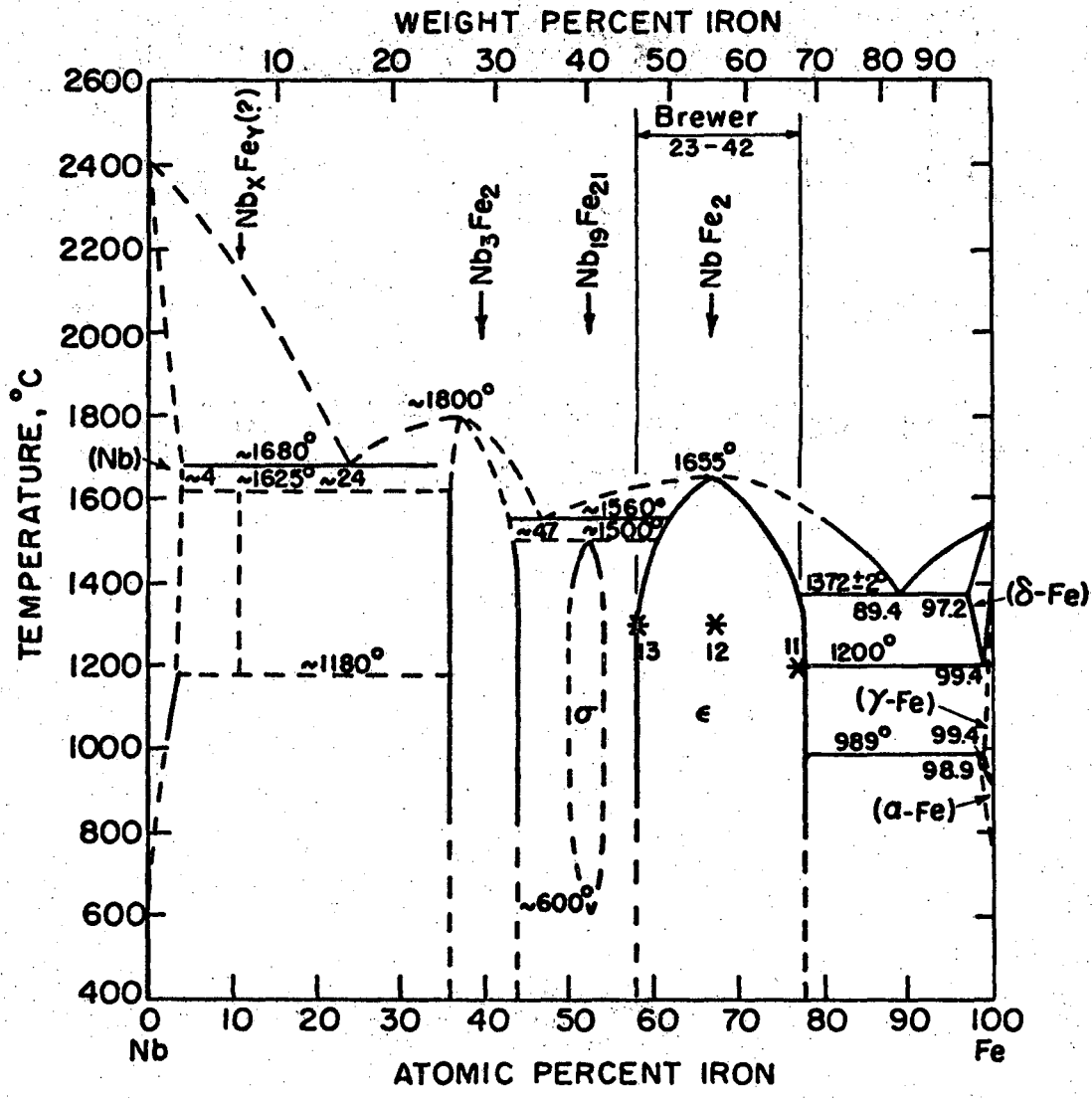

XBL 7012-7237

Figure 1

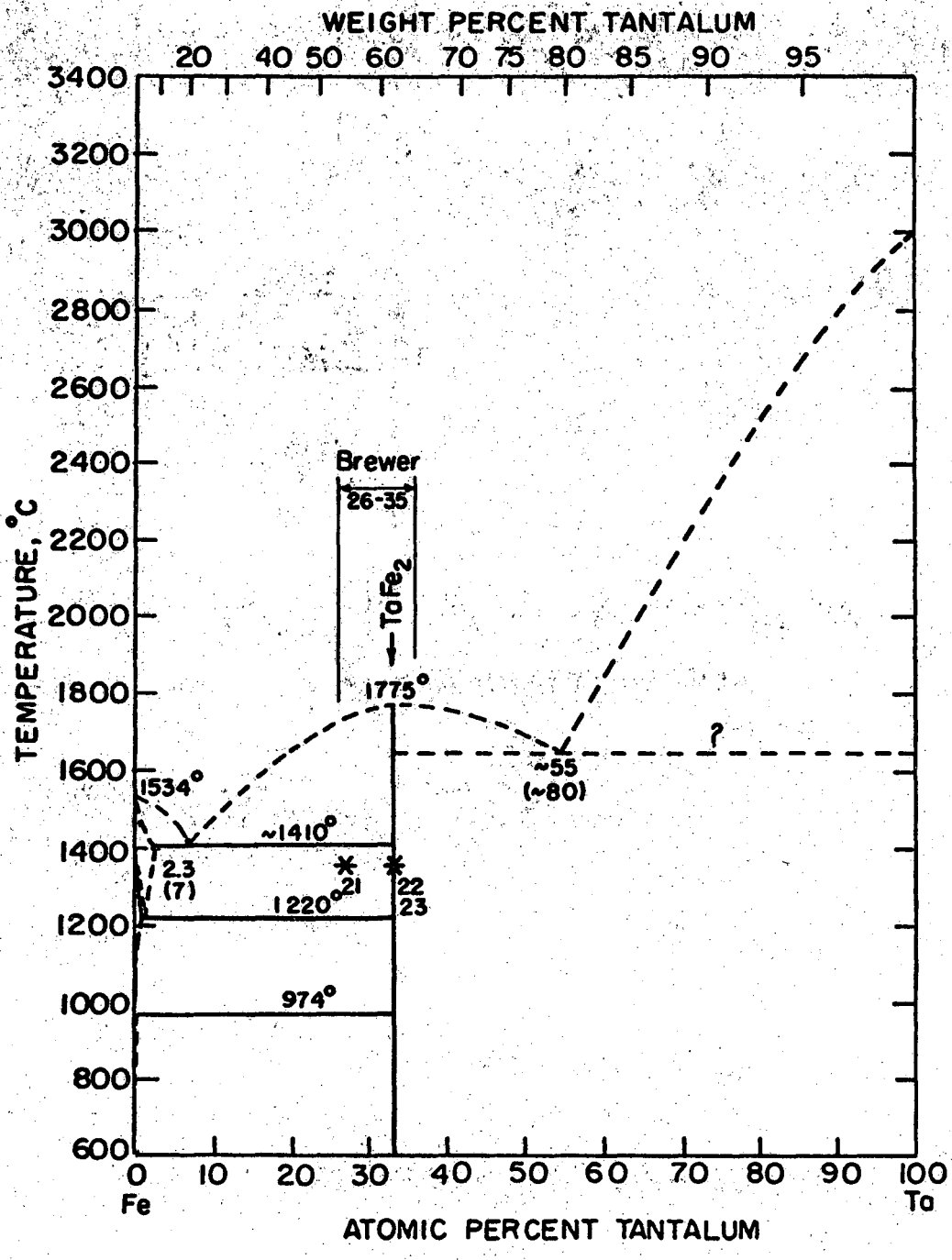

XBL 7012-7238

Figure 2

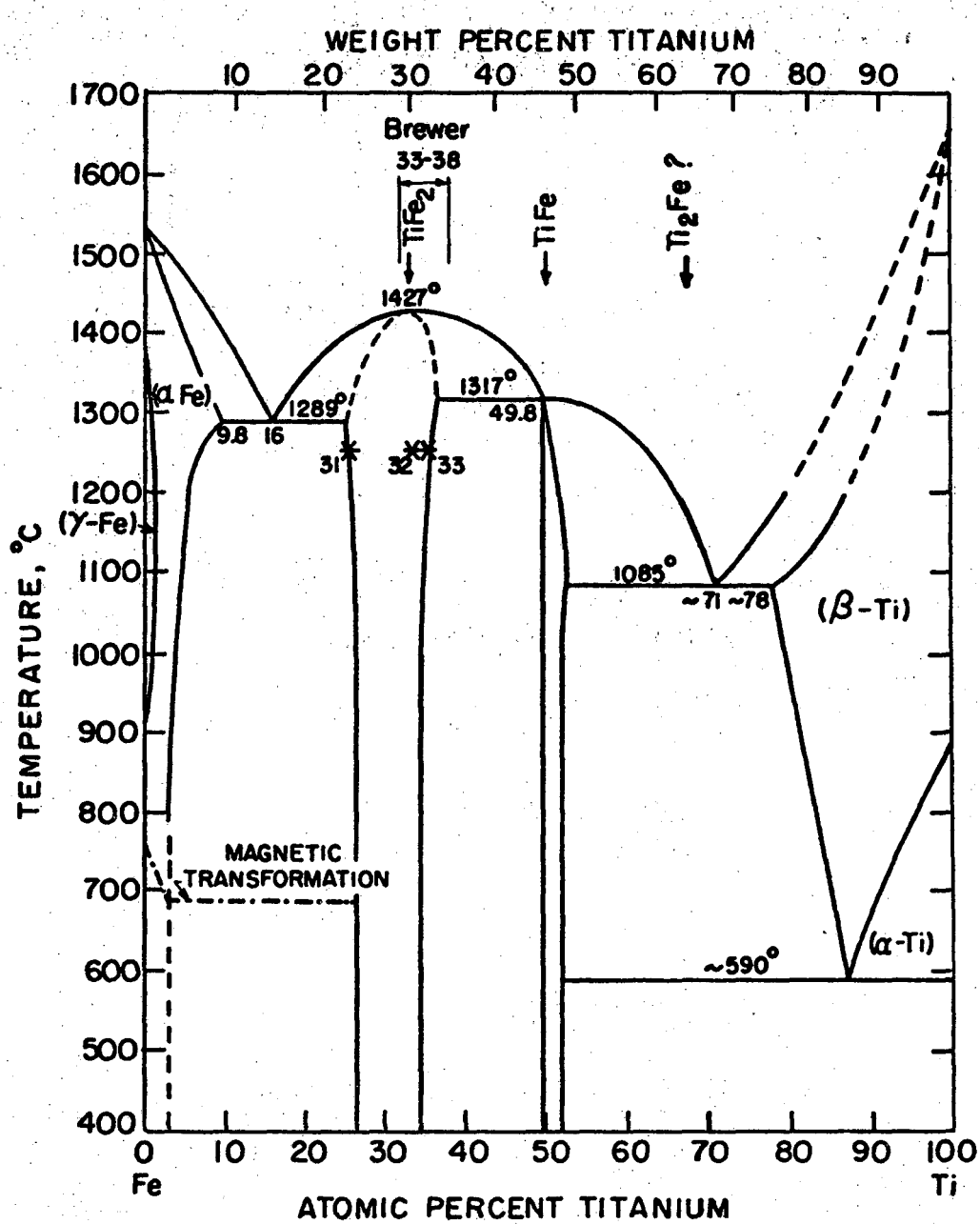

XBL 7012-7239

Figure 3

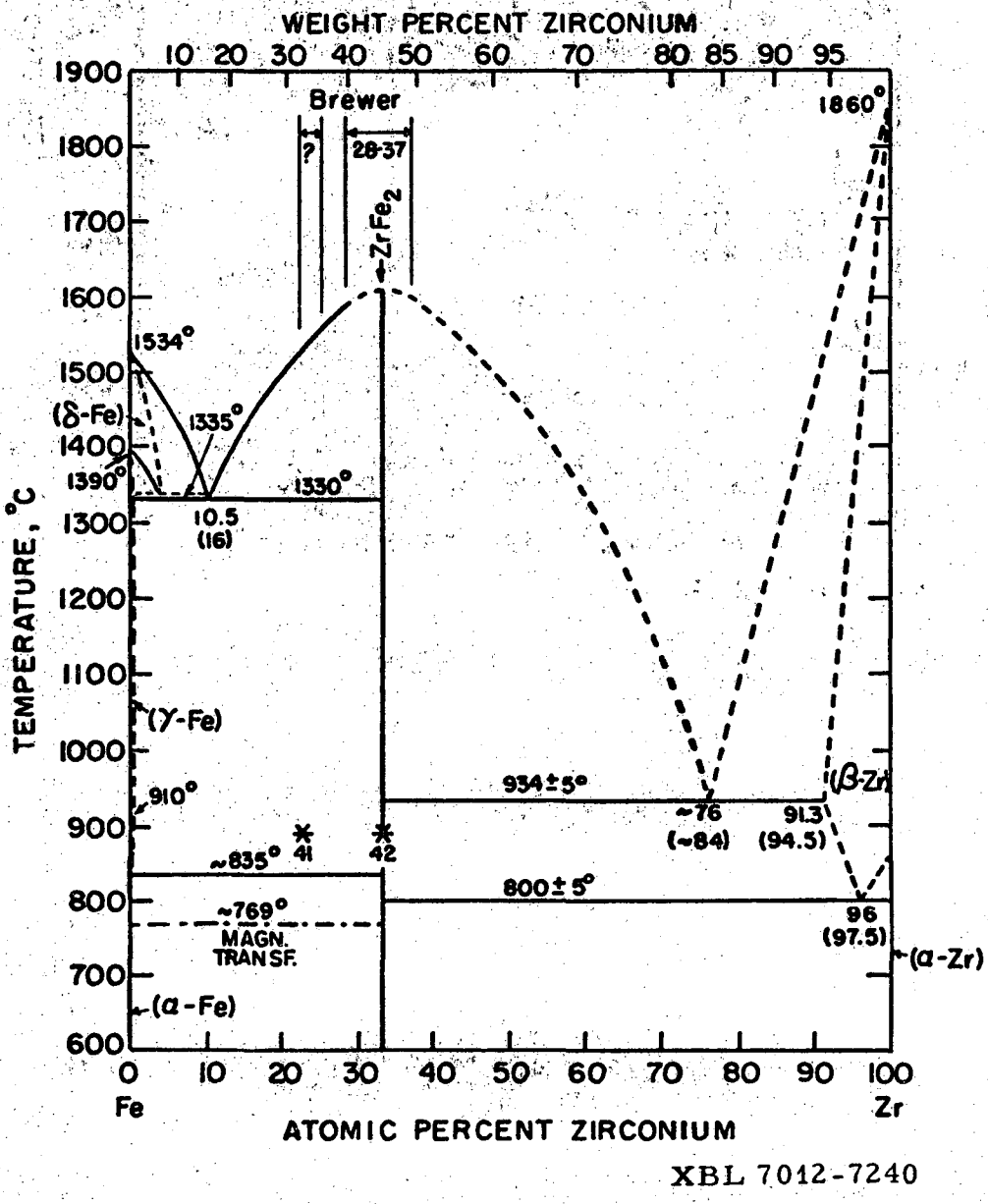
WEIGHT PERCENT ZIRCONIUM
10 20 30 40 50 60 70 80 85 90 95
1900
1800
1700
1600
1500
1400
1300
1200
1100
1000
900
800
700
600
TEMPERATURE, °C
Brewer
?
28-37
ZrFe2
1860°
1534°
(δ-Fe)
1335°
1390°
1330°
10.5
(16)
(γ-Fe)
910°
934±5°
~76
(~84)
91.3
(94.5)
(β-Zr)
~835°
41
42
800±5°
96
(97.5)
(α-Zr)
~769°
MAGN.
TRANSF.
(α-Fe)
0 10 20 30 40 50 60 70 80 90 100
Fe
Zr
ATOMIC PERCENT ZIRCONIUM
XBL 7012-7240

Figure 4

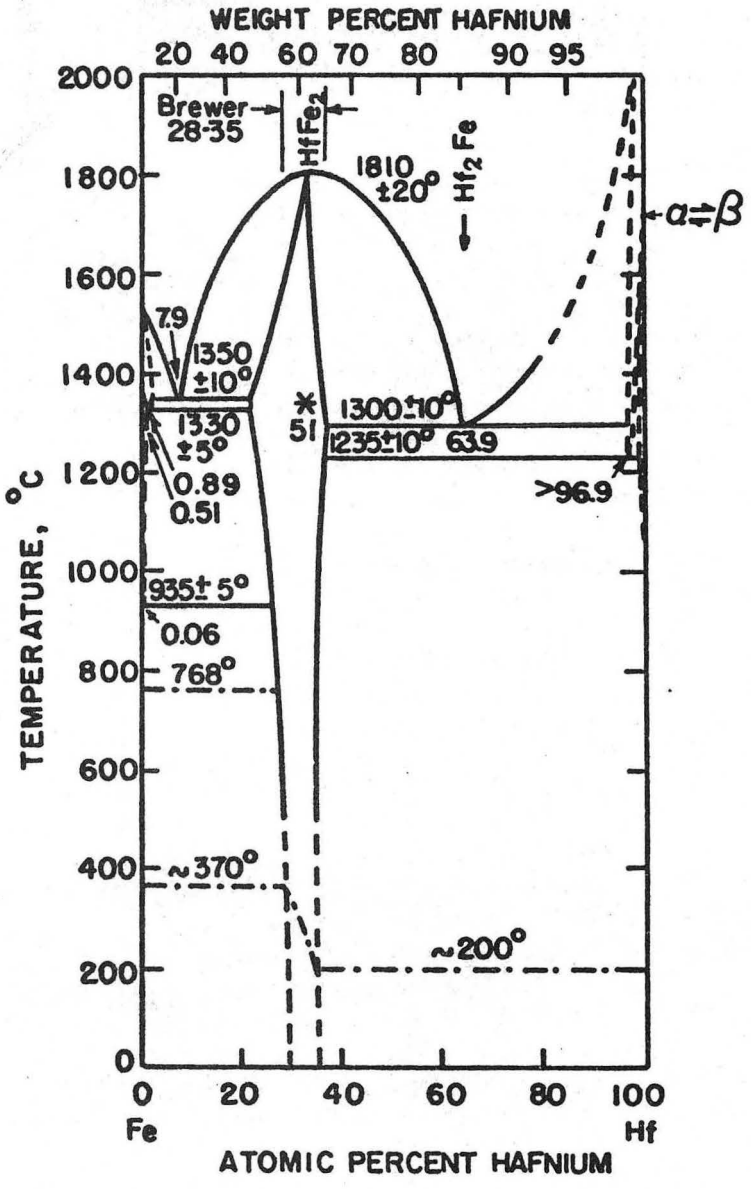

XBL 7012-7241

Figure 5

(a)

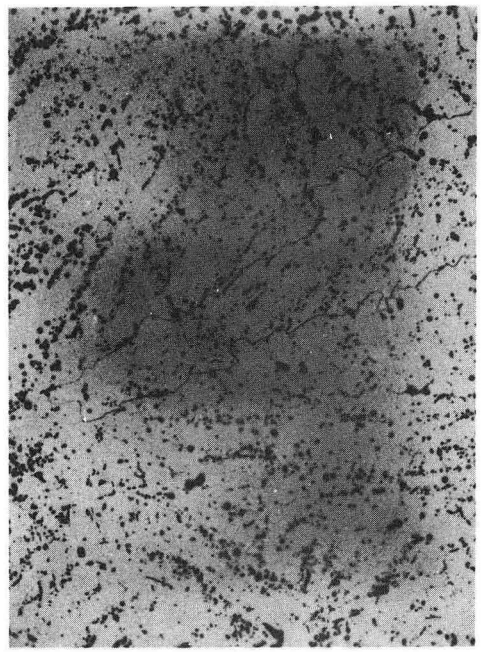

(b)

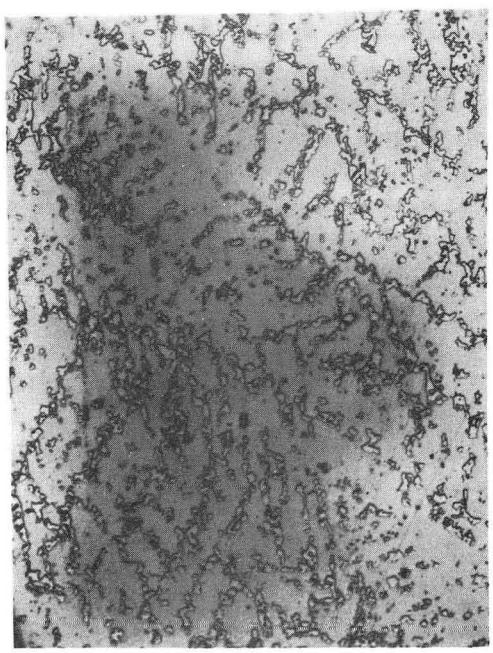

(c)

XBB7012-5409

Figure 6

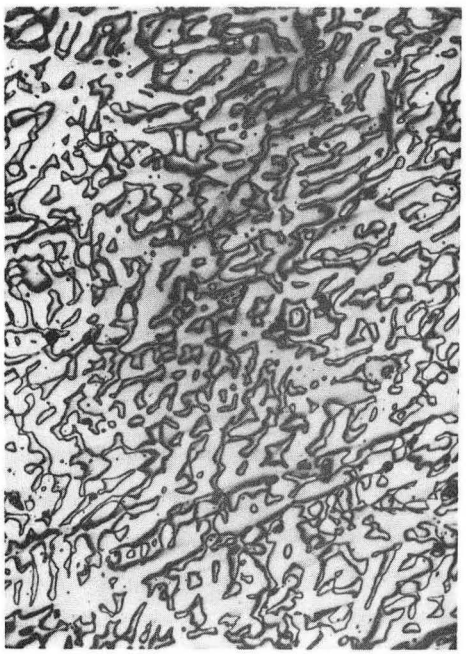

(a)

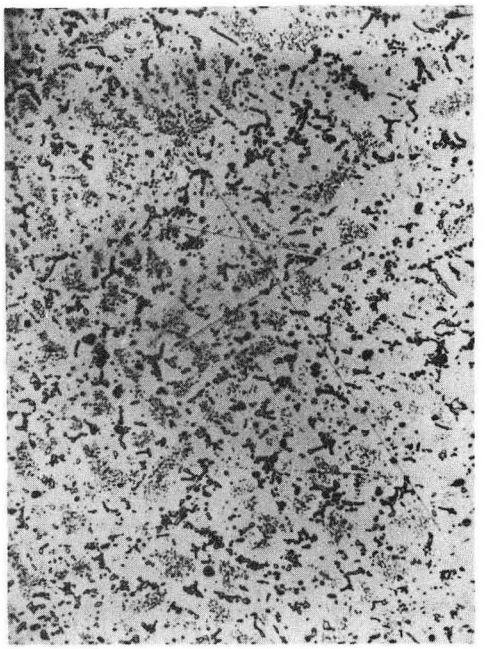

(b)

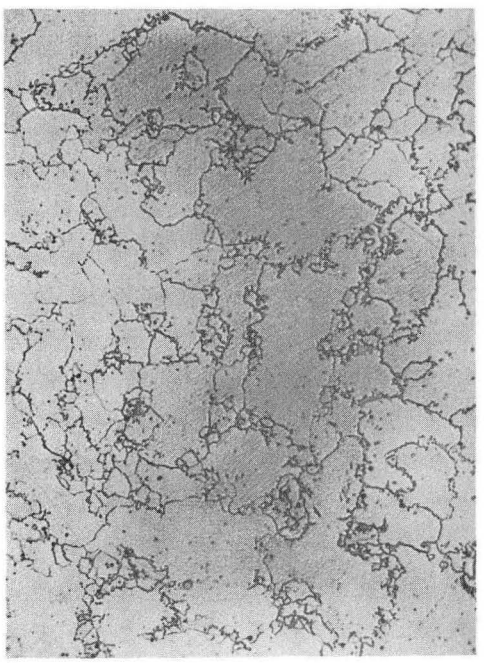

(c)

XBB7012-5408

Figure 7

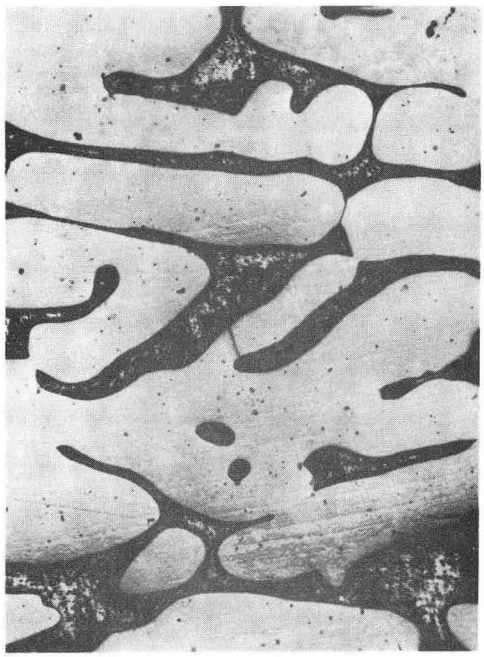

(a)

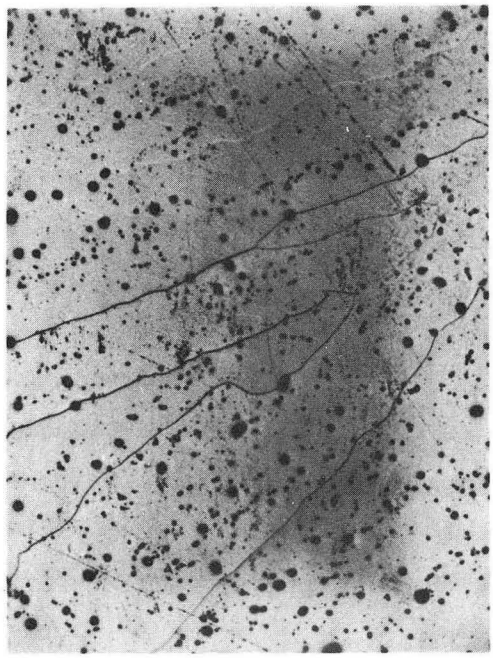

(b)

(c)

XBB7012-5410

Figure 8

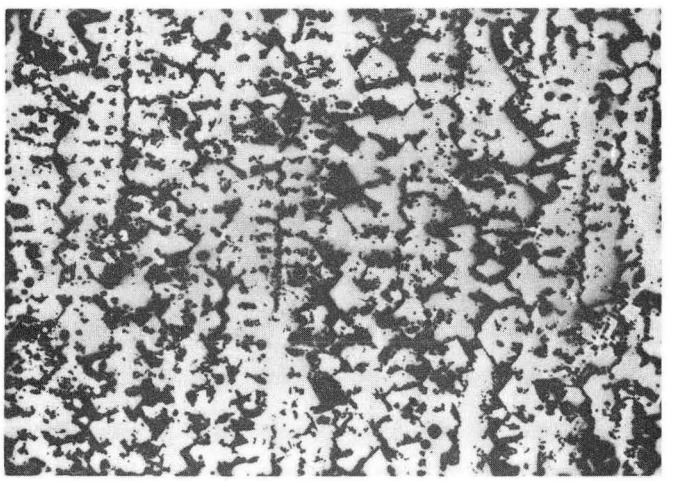

(a)

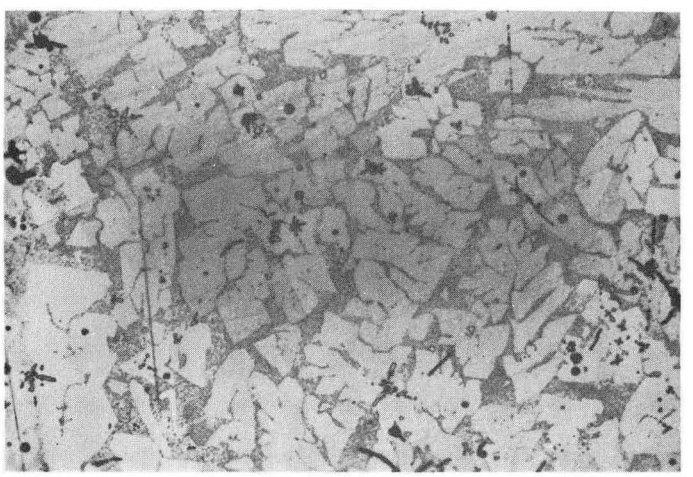

(b)

XBB7012-5407

Figure 9

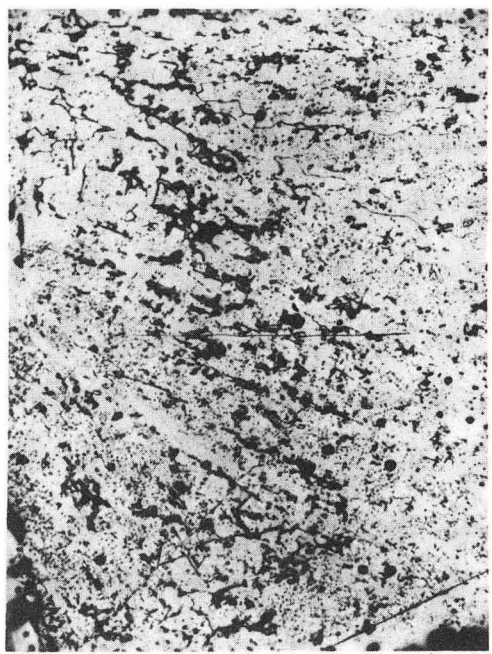

XBB7012-5406

Figure 10

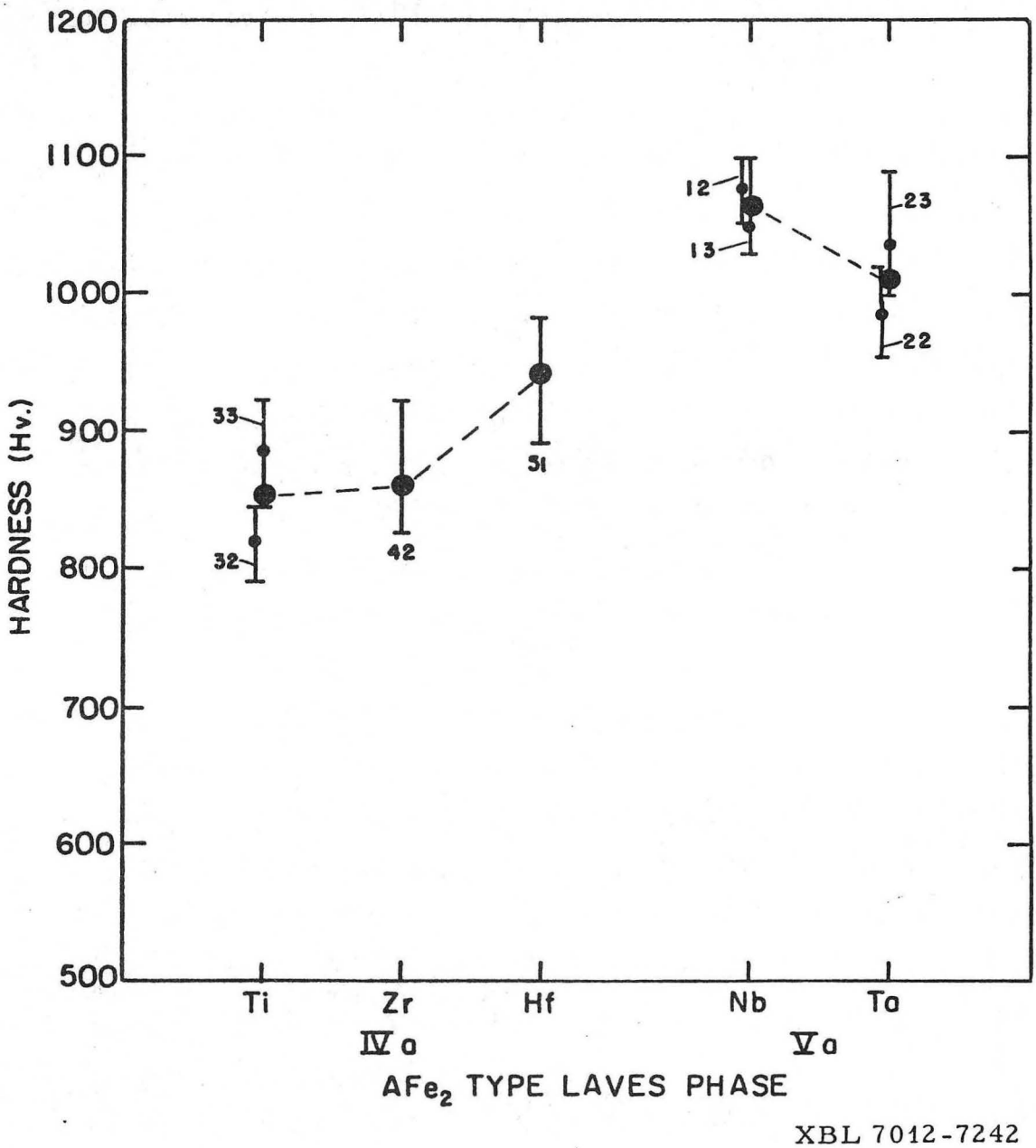

XBL 7012-7242

Figure 11

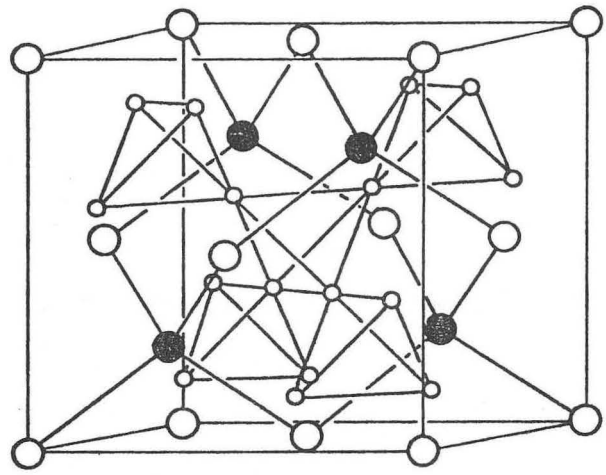

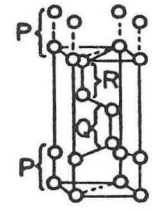

Figure 12

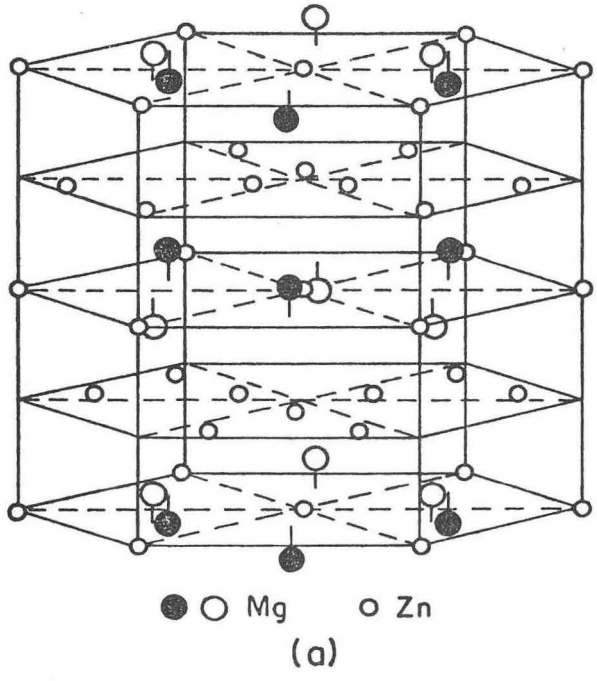

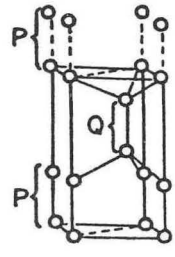

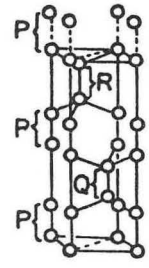

XBL 7012-7243

Figure 13

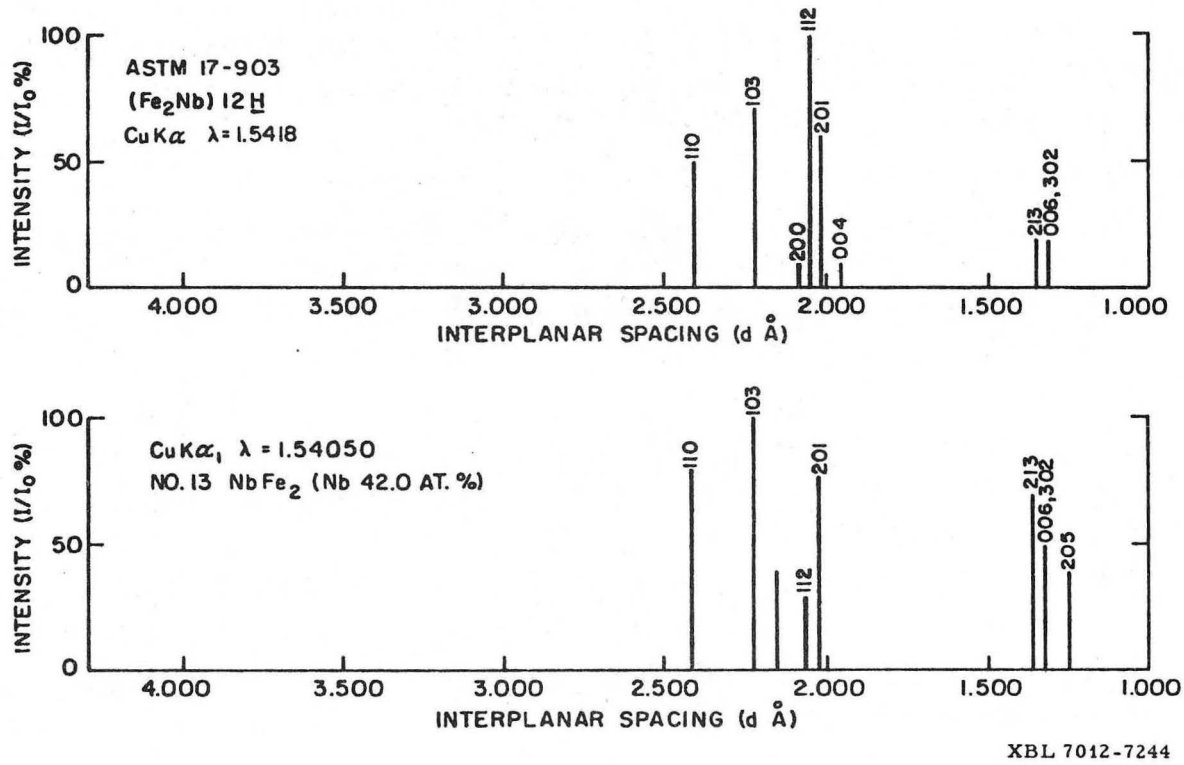
100
50
0
INTENSITY (I/I₀ %)
ASTM 17-903
(Fe₂Nb) 12 H
CuKα λ=1.5418
110
103
112
201
200
004
213
006, 302
4.000
3.500
3.000
2.500
2.000
1.500
1.000
INTERPLANAR SPACING (d Å)
CuKα₁ λ = 1.54050
NO. 13 NbFe₂ (Nb 42.0 AT. %)
110
103
201
112
213
006,302
205
INTERPLANAR SPACING (d Å)
XBL 7012-7244

Figure 14

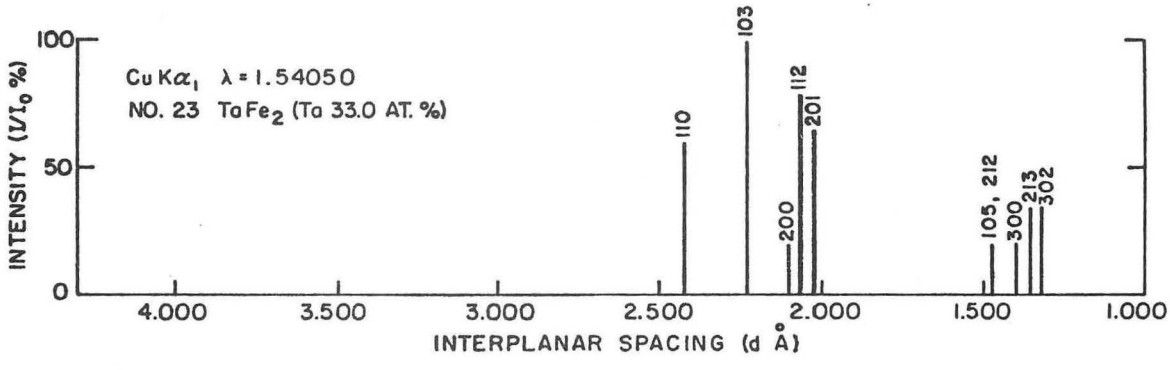

XBL 7012-7245

Figure 15

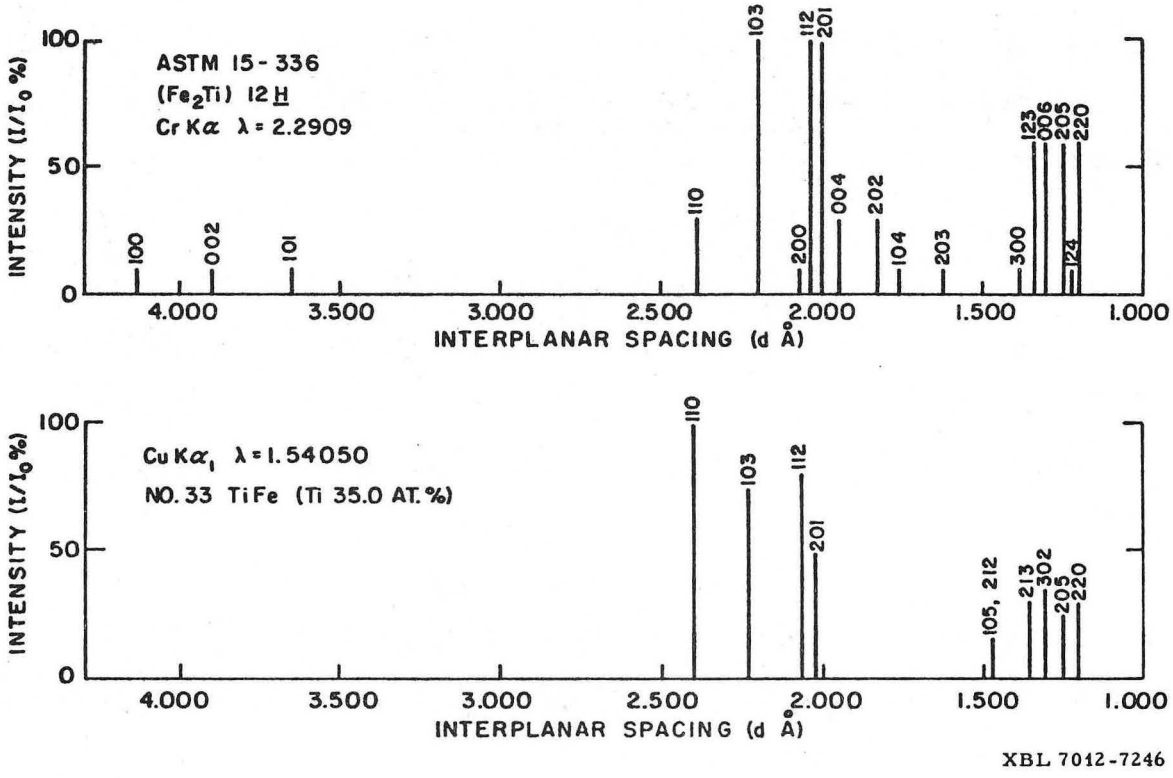
ASTM 15-336
(Fe2Ti) 12H
Cr Kα λ = 2.2909
INTENSITY (I/I0 %)
INTERPLANAR SPACING (d Å)
100
002
101
110
103
112
201
200
004
202
104
203
300
123
006
205
220
124
CuKα1 λ = 1.54050
NO. 33 TiFe (Ti 35.0 AT.%)
105, 212
213
302
XBL 7012-7246

Figure 16

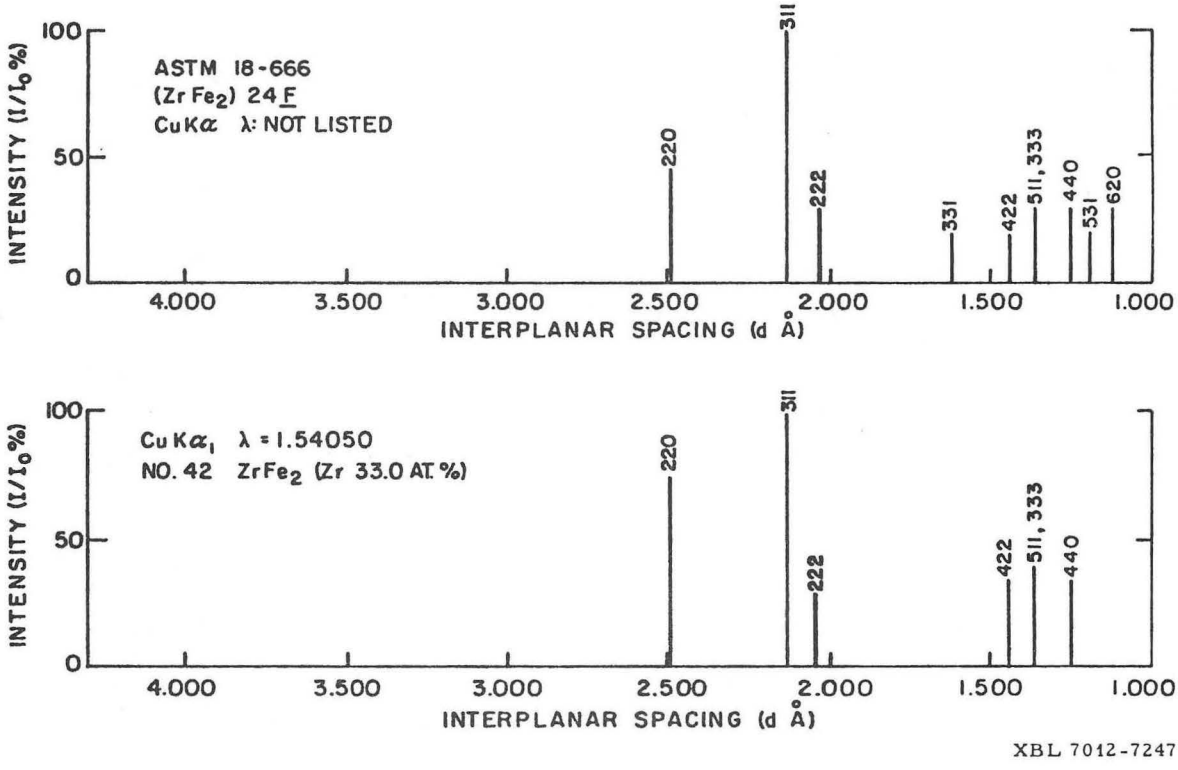
INTENSITY (I/I₀ %)
100
50
0
ASTM 18-666
(Zr Fe₂) 24 F
CuKα λ: NOT LISTED
220
311
222
331
422
511, 333
440
531
620
4.000
3.500
3.000
2.500
2.000
1.500
1.000
INTERPLANAR SPACING (d Å)
INTENSITY (I/I₀ %)
100
50
0
CuKα₁ λ = 1.54050
NO. 42 ZrFe₂ (Zr 33.0 AT. %)
220
311
222
422
511, 333
440
4.000
3.500
3.000
2.500
2.000
1.500
1.000
INTERPLANAR SPACING (d Å)
XBL 7012-7247

Figure 17

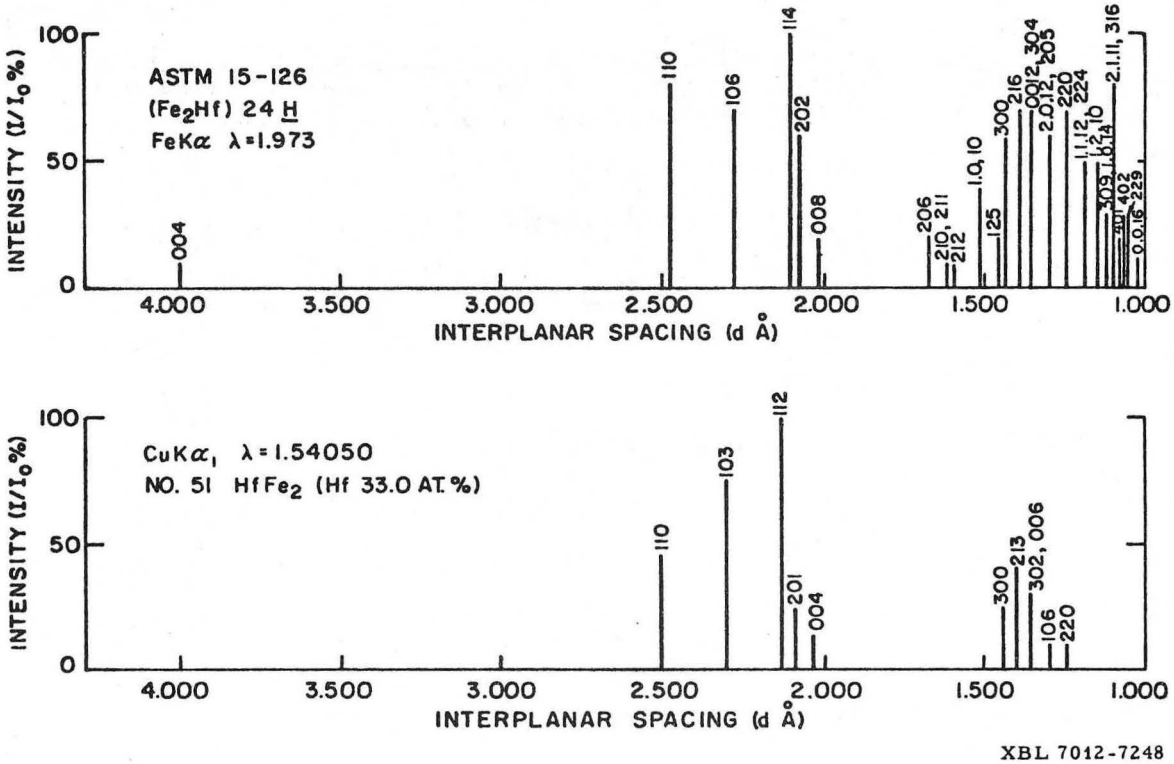
ASTM 15-126
(Fe2Hf) 24 H
FeKα λ=1.973
INTENSITY (I/I0 %)
INTERPLANAR SPACING (d Å)
CuKα1 λ=1.54050
NO. 51 HfFe2 (Hf 33.0 AT.%)
XBL 7012-7248

Figure 18

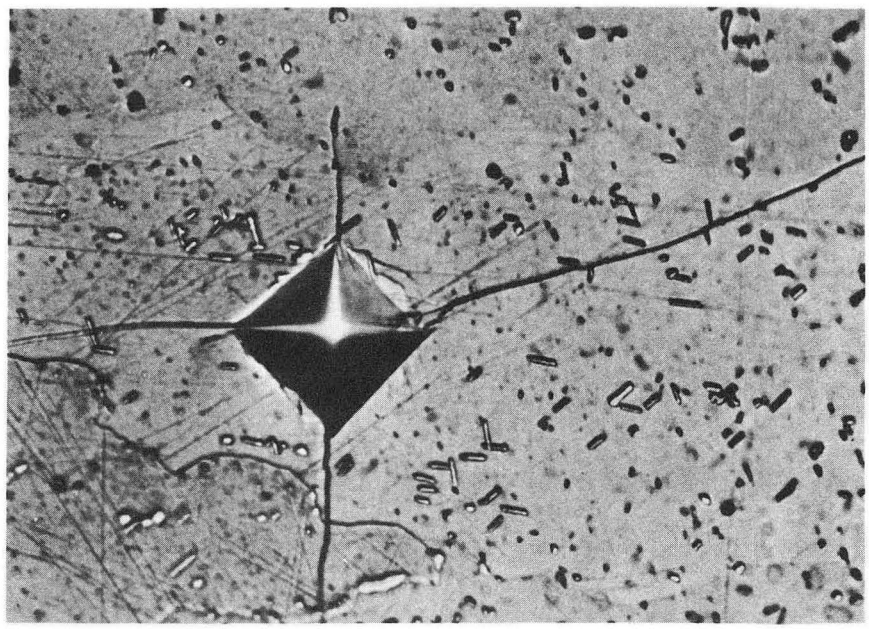

XBB7012-5422

Figure 19

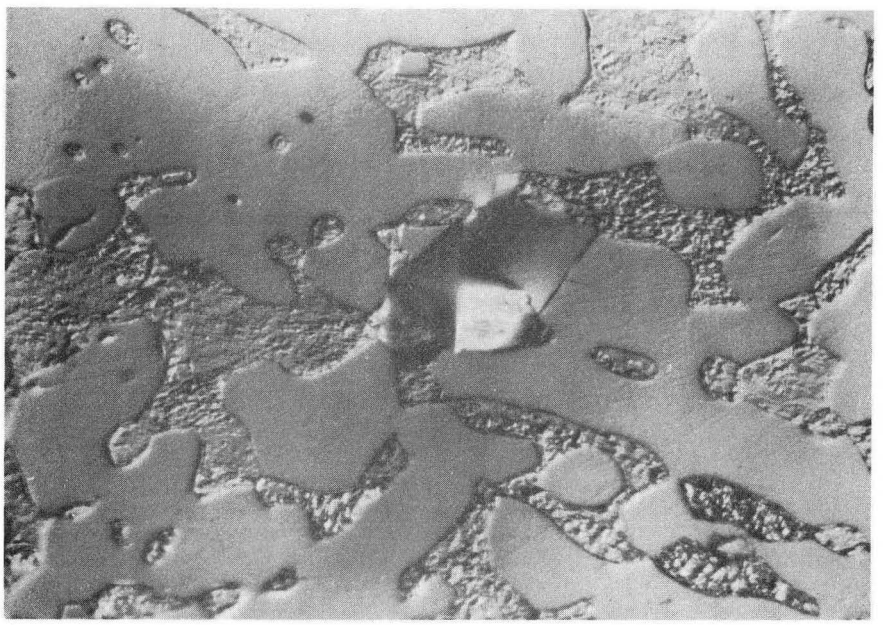

(a)

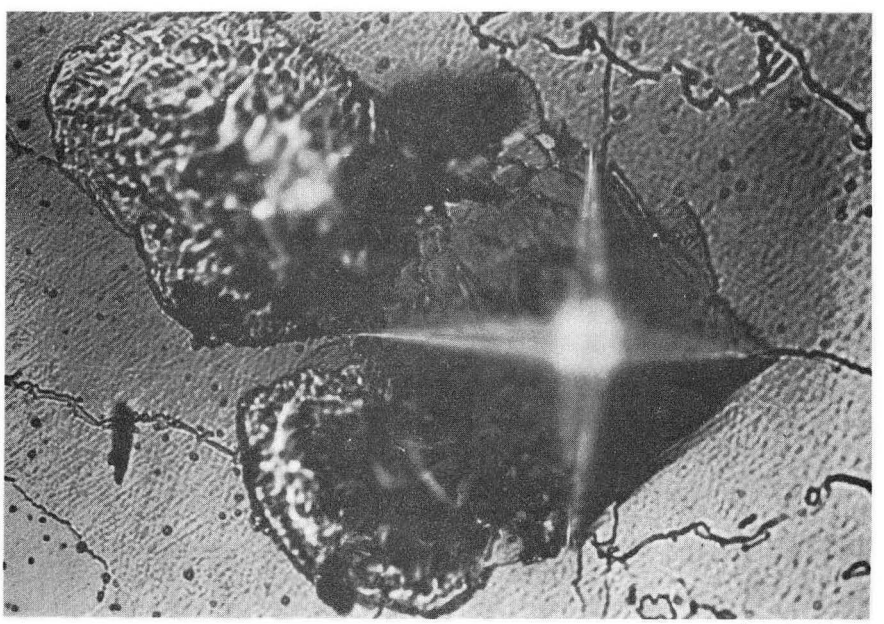

(b)

XBB7012-5425

Figure 20

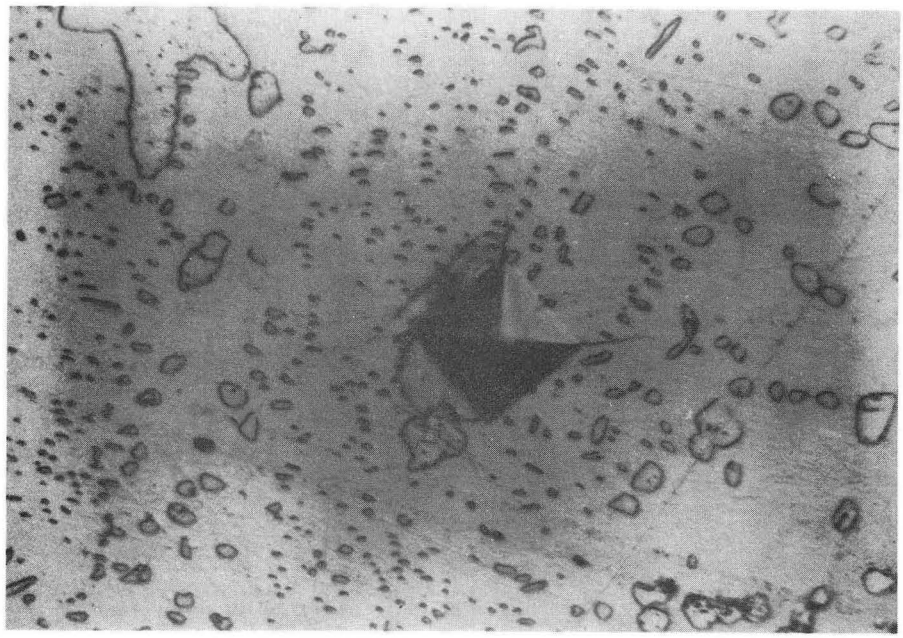

Figure 21

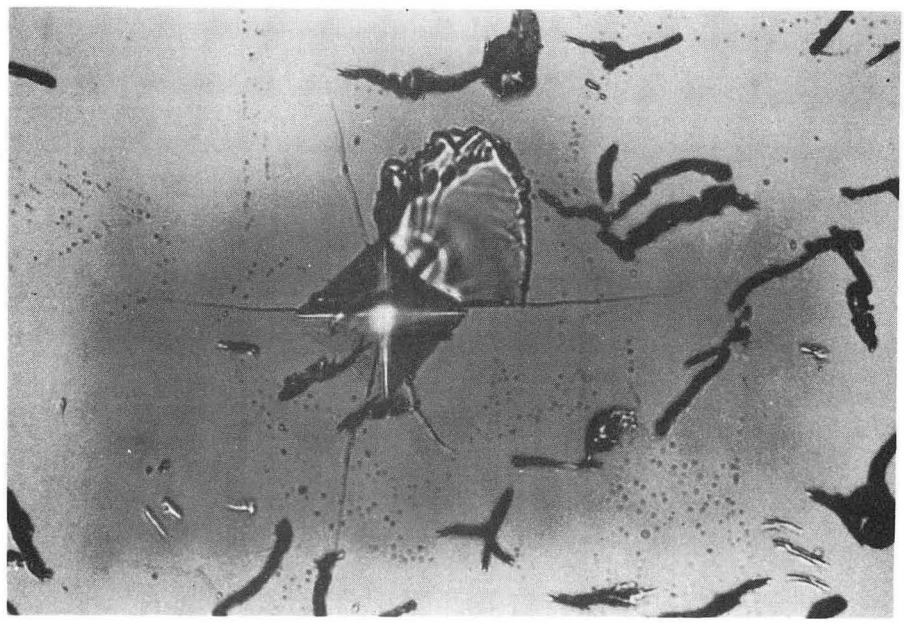

Figure 22 XBB7012-5419

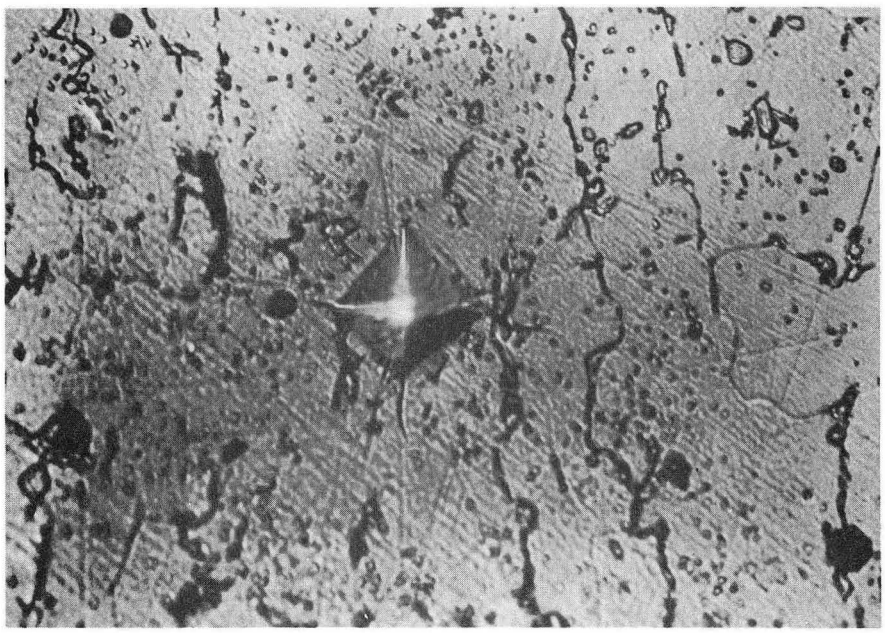

XBB7012-5420

Figure 23

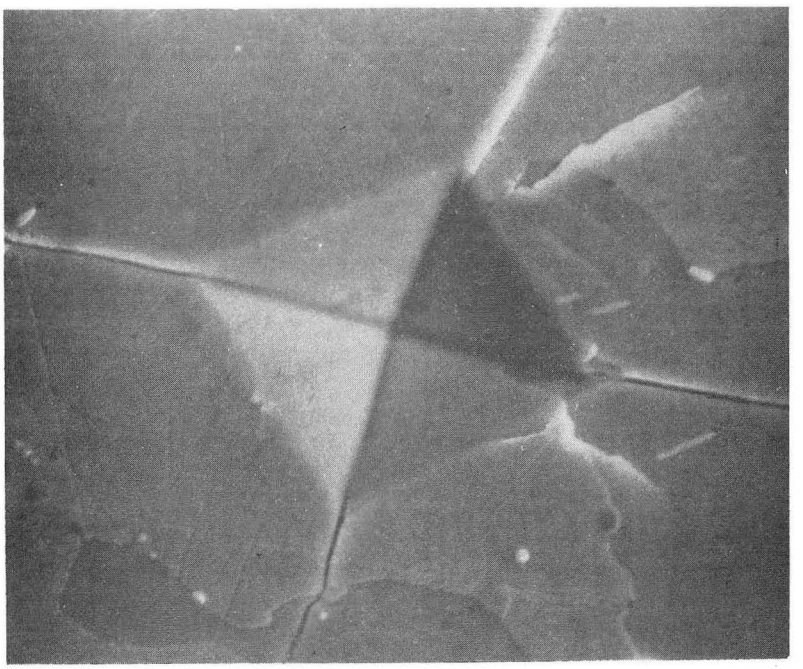

(a)

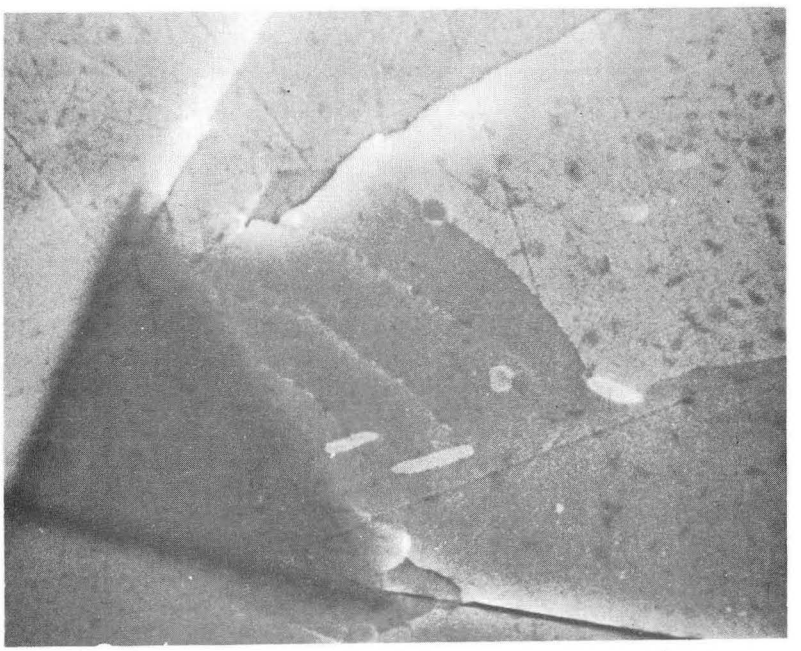

(b) XBB7012-5415

Figure 24

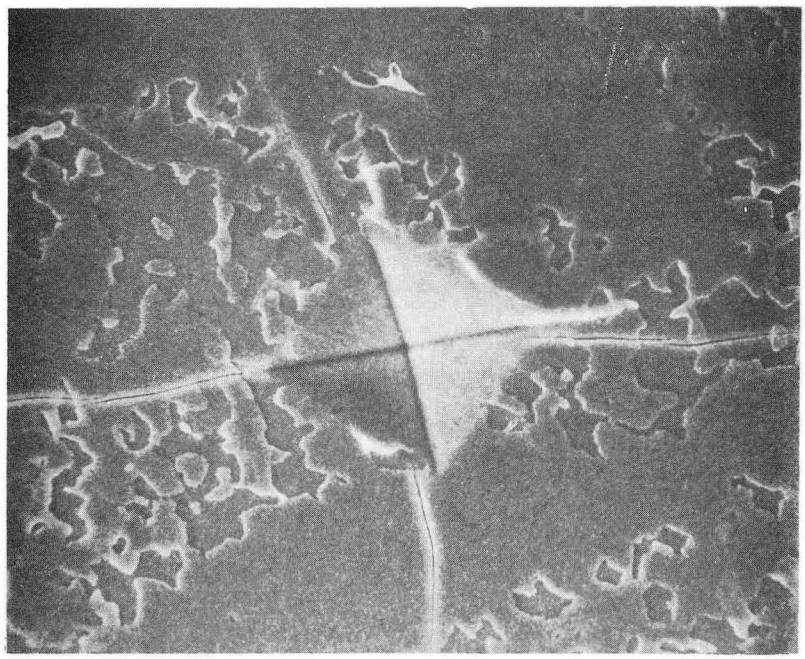

(a)

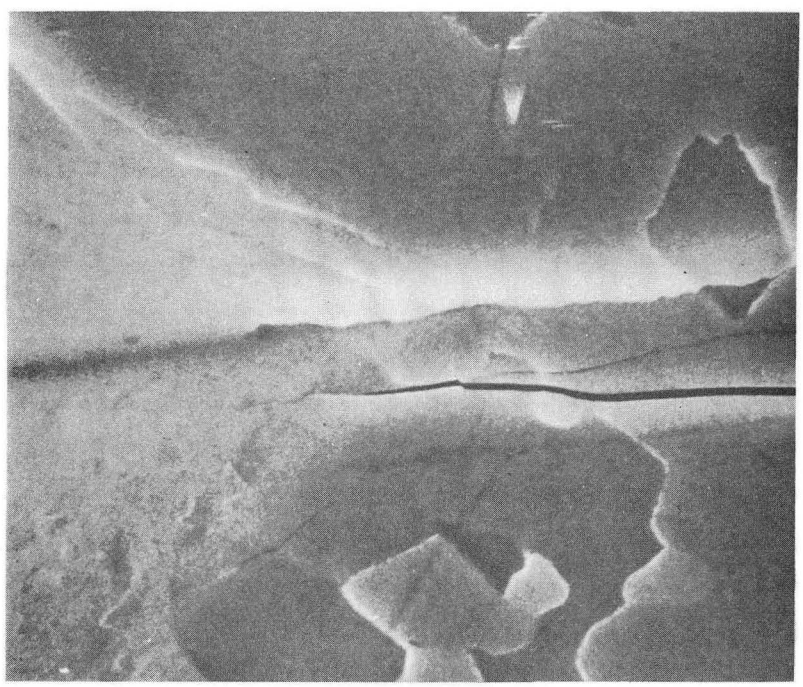

(b)

XBB7012-5414

Figure 25

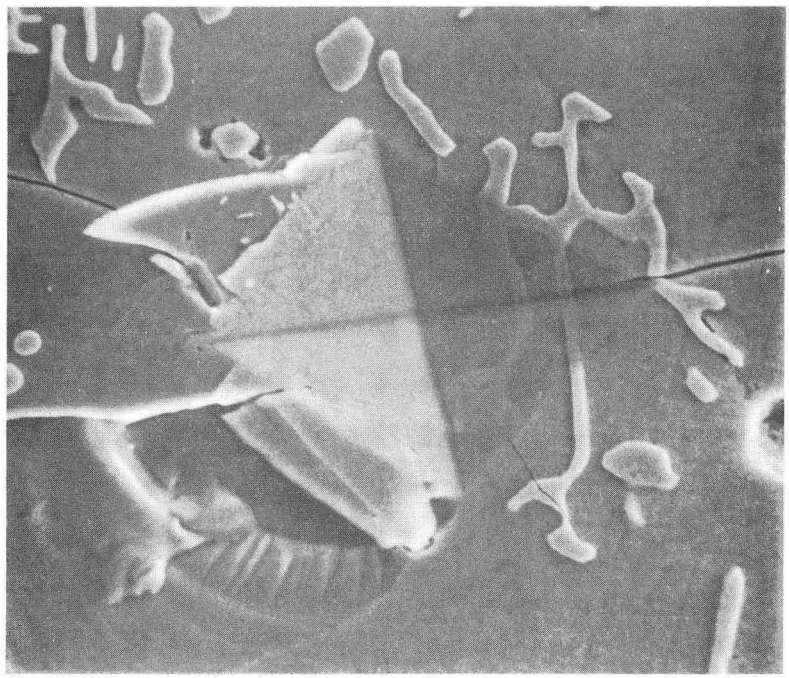

(a)

(b)

XBB7012-5417

Figure 26

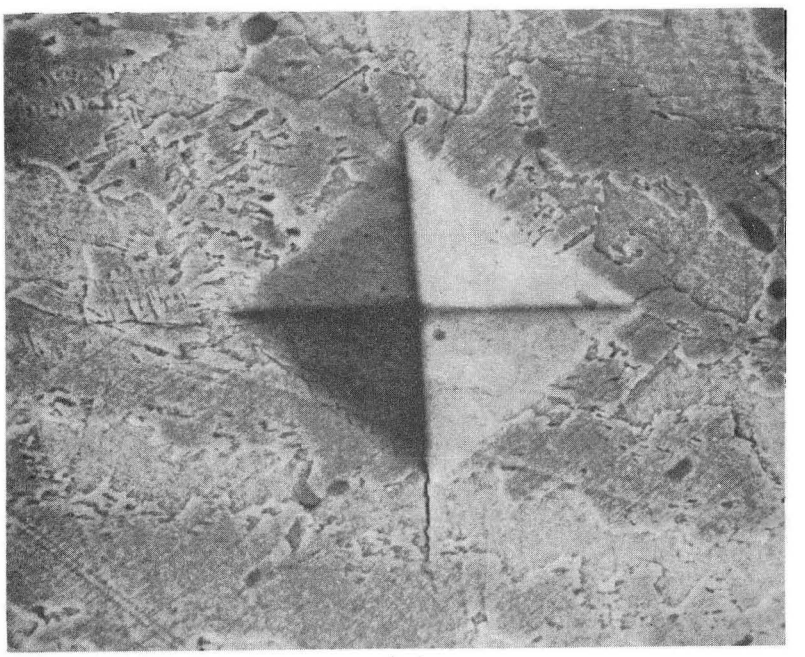

(a)

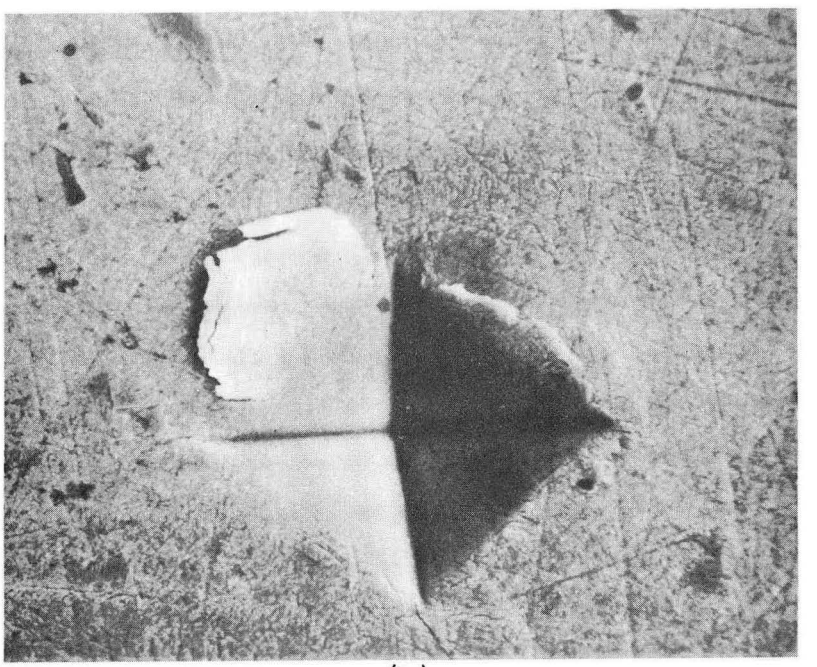

(b)

XBB7012-5424

Figure 27

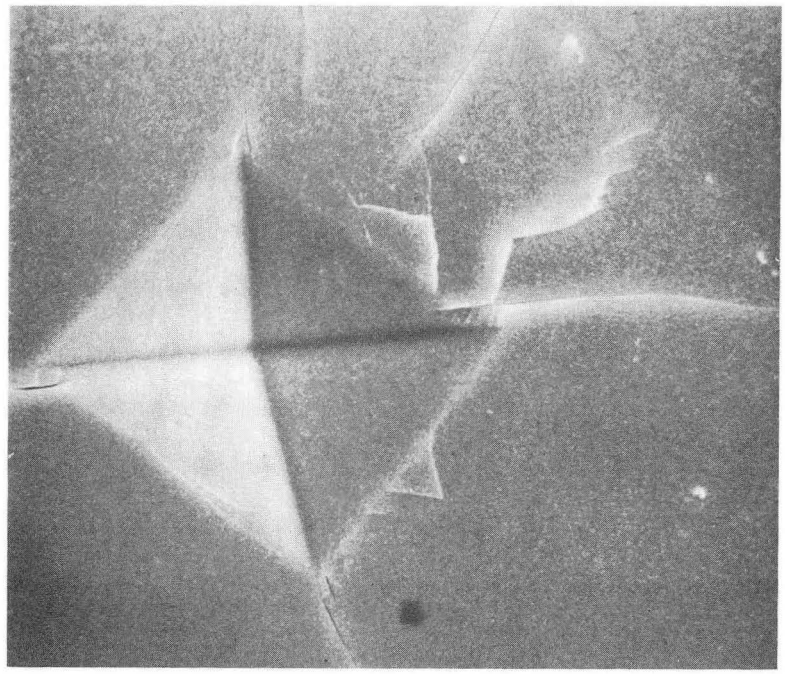

(a)

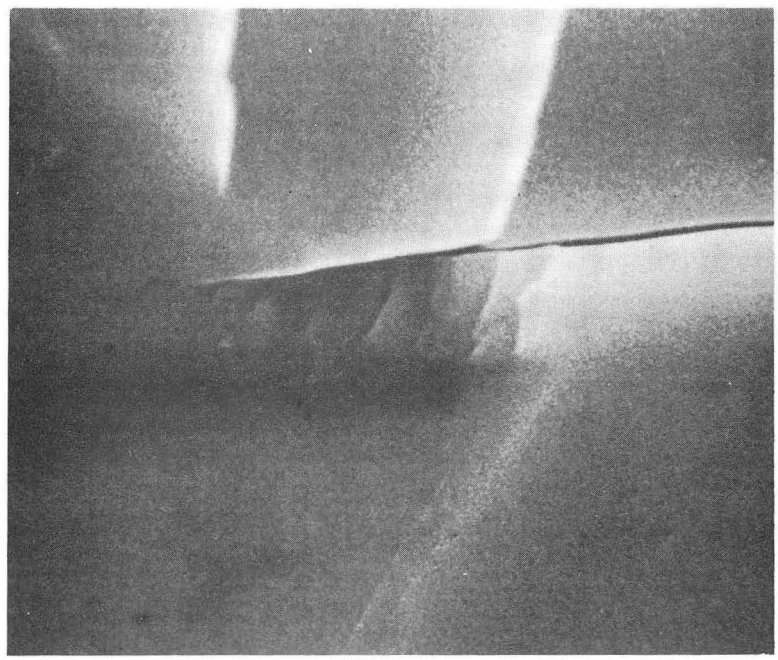

(b)

XBB7012-5426

Figure 28

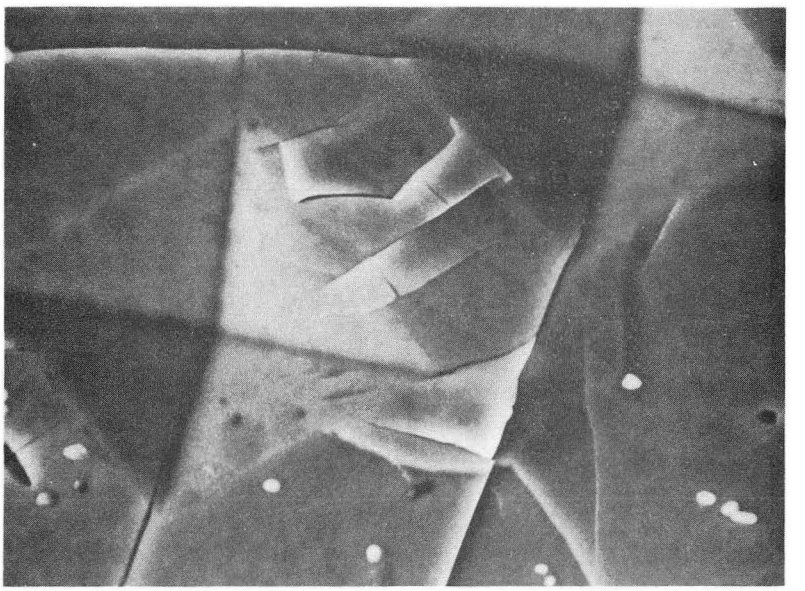

(a)

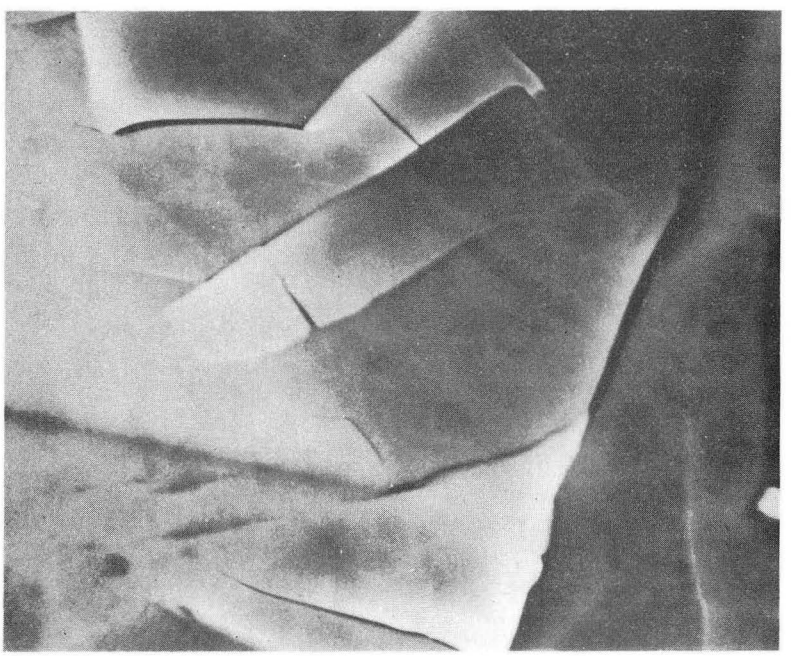

(b) XBB7012-5428

Figure 29

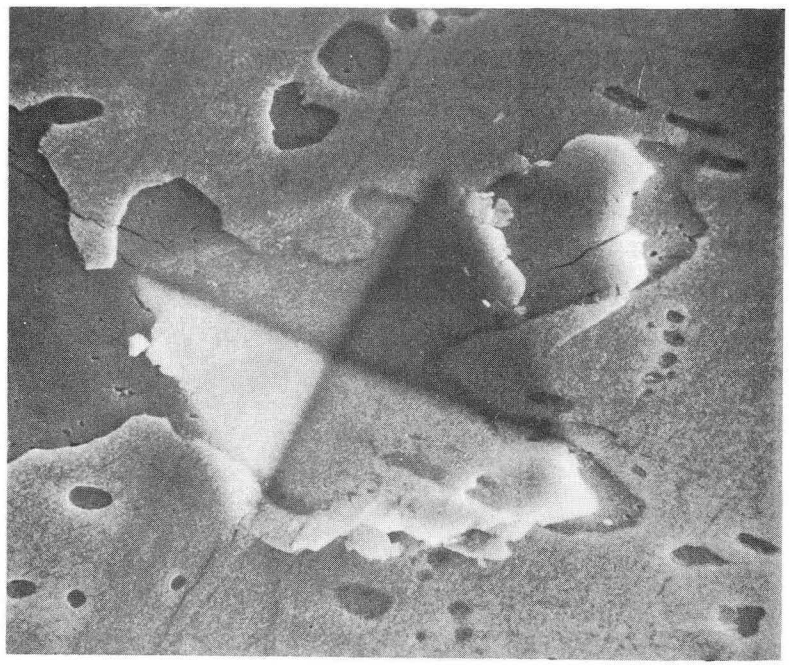

(a)

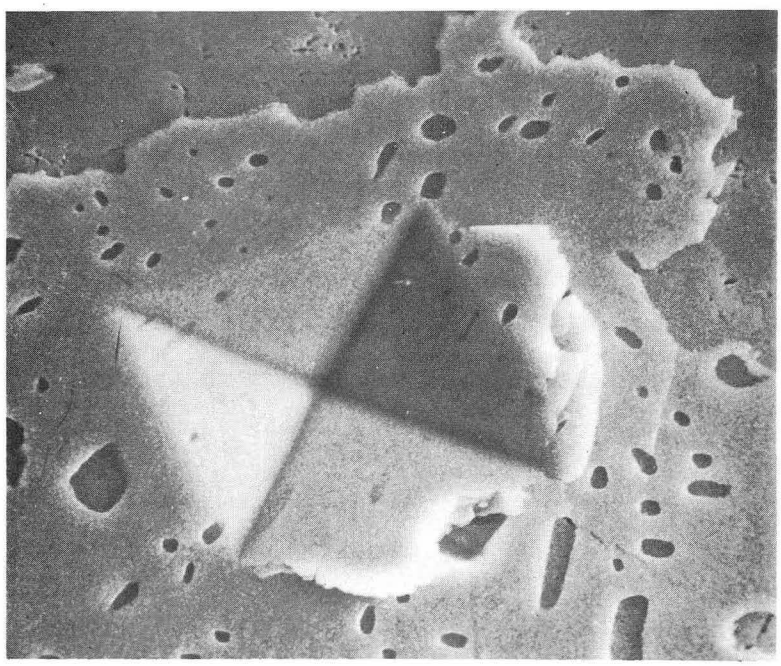

(b) XBB7012-5423

Figure 30

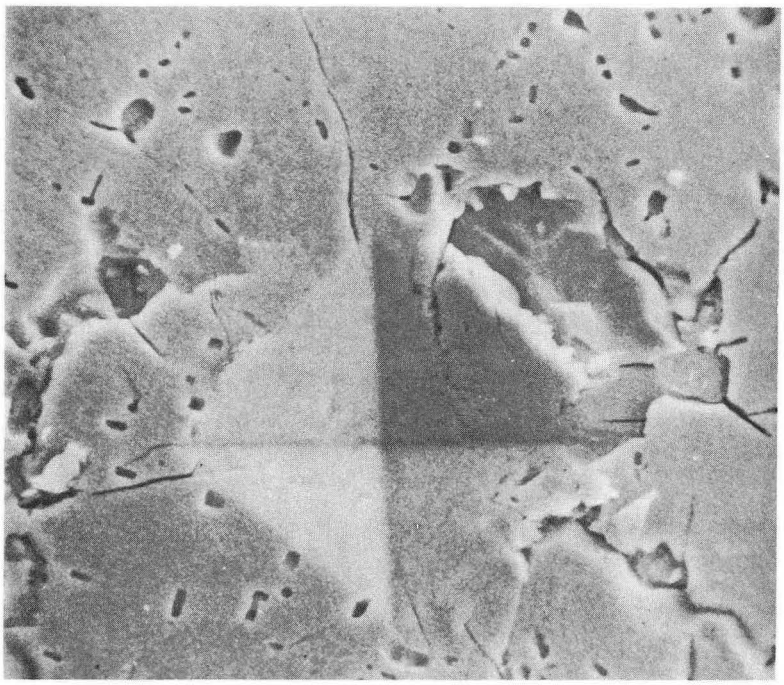

(a)

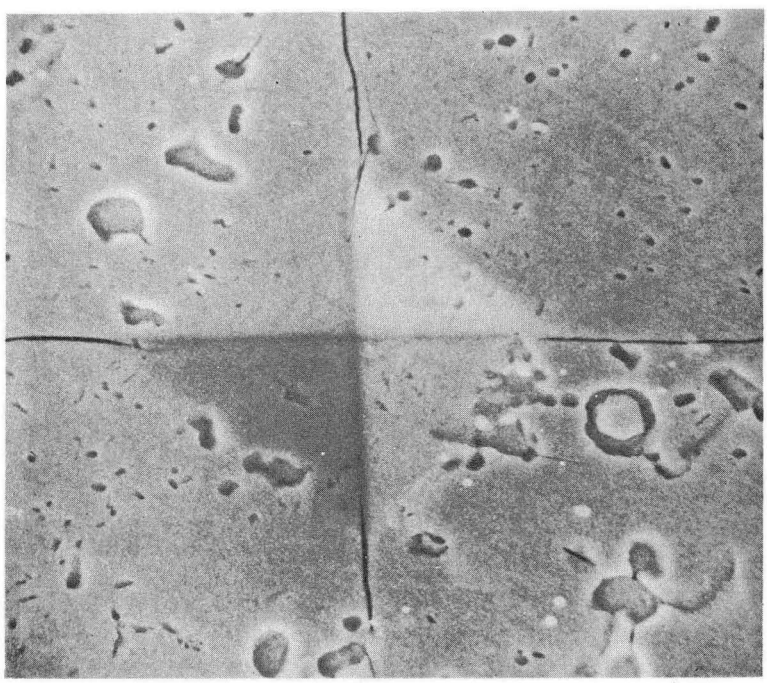

(b) XBB7012-5427

Figure 31

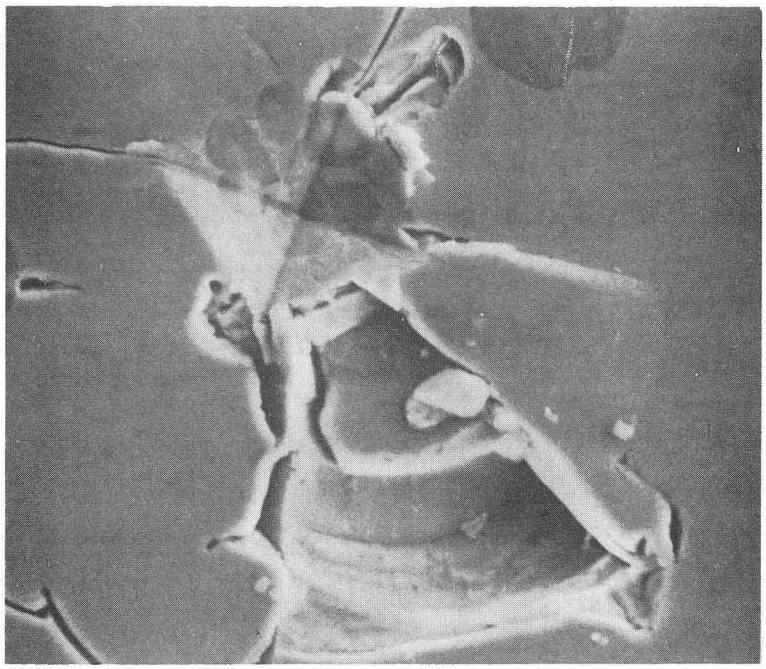

(a)

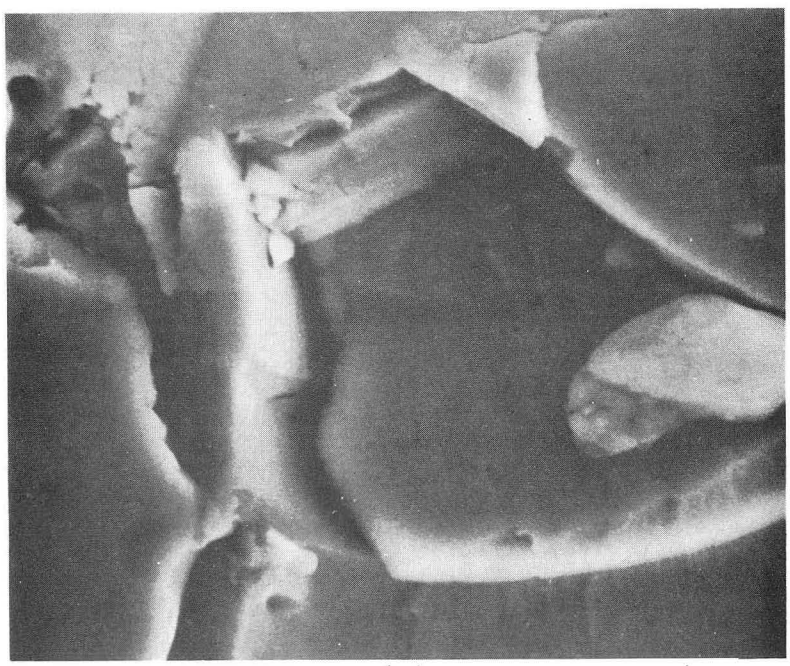

(b) XBB7012-5413

Figure 32

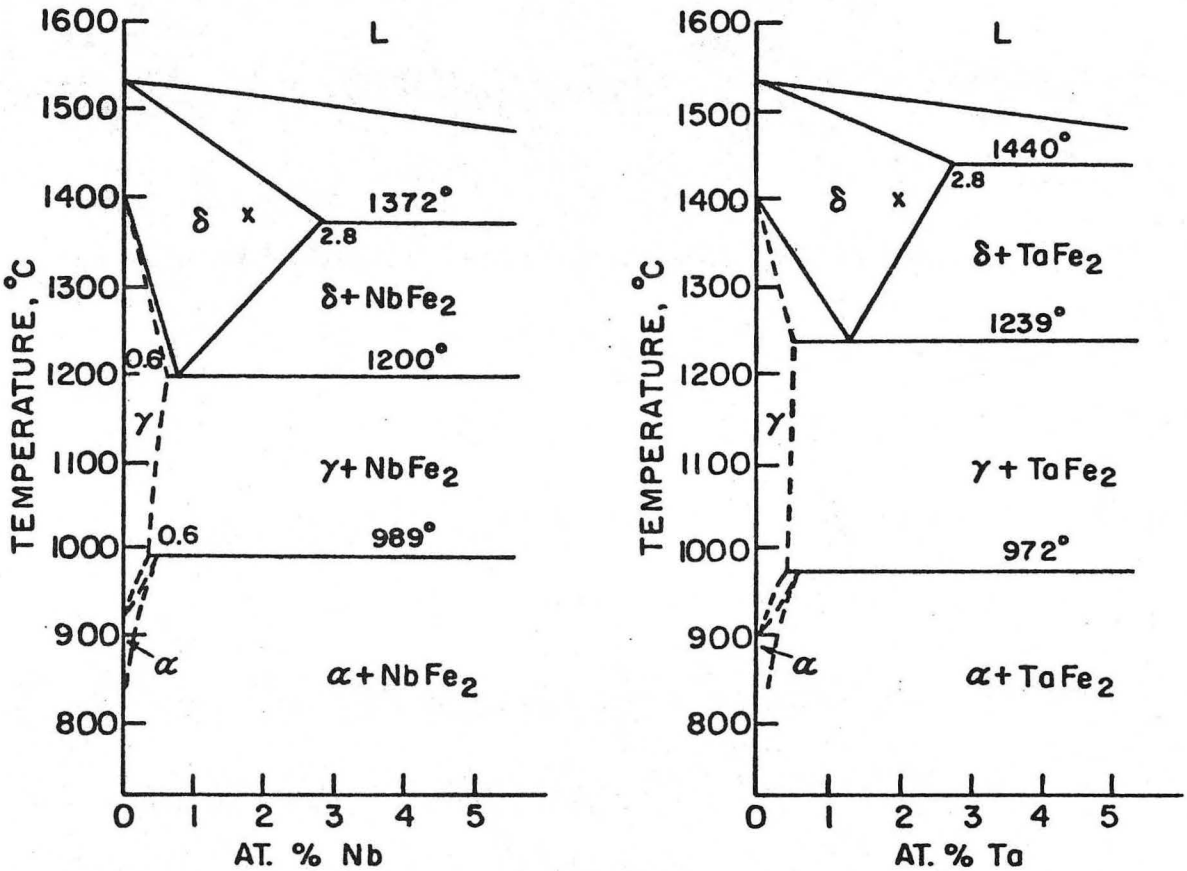
1600
1500
1400
1300
1200
1100
1000
900
800
TEMPERATURE, °C
L
δ x
1372°
2.8
δ+NbFe2
1200°
0.6
γ
γ+NbFe2
0.6
989°
α
α+NbFe2
0 1 2 3 4 5
AT. % Nb
1600
1500
1400
1300
1200
1100
1000
900
800
TEMPERATURE, °C
L
1440°
2.8
δ x
δ+TaFe2
1239°
γ
γ+TaFe2
972°
α
α+TaFe2
0 1 2 3 4 5
AT. % Ta
XBL 7012-7250

Figure 33

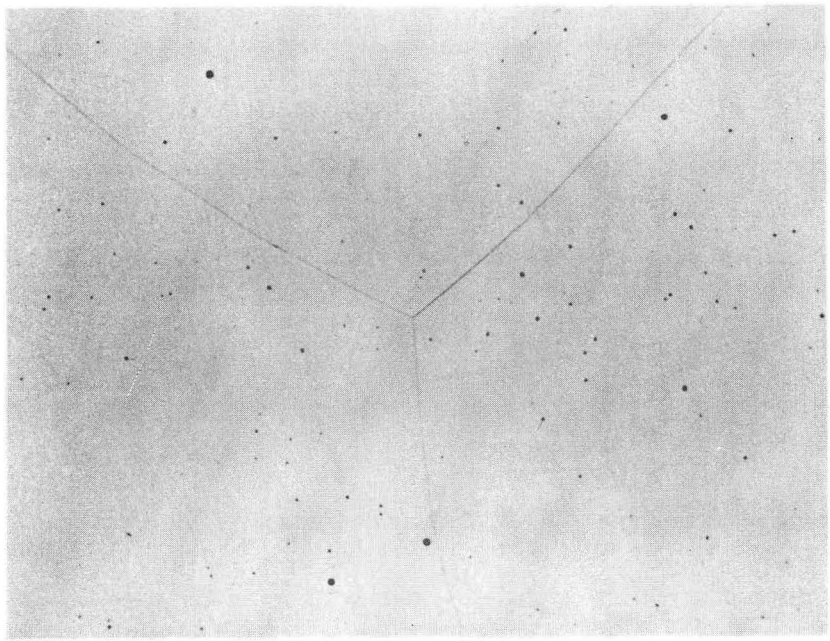

(a)

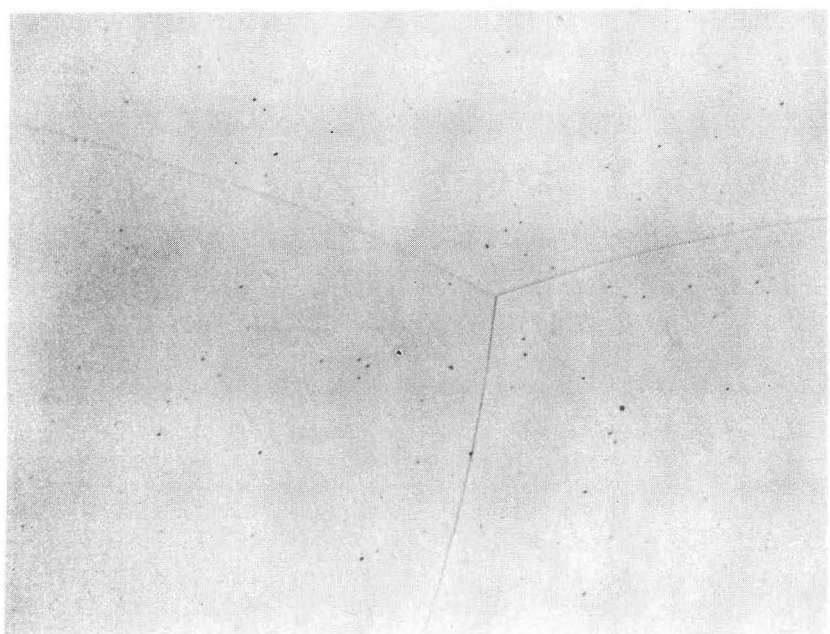

(b) XBB7012-5421

Figure 34

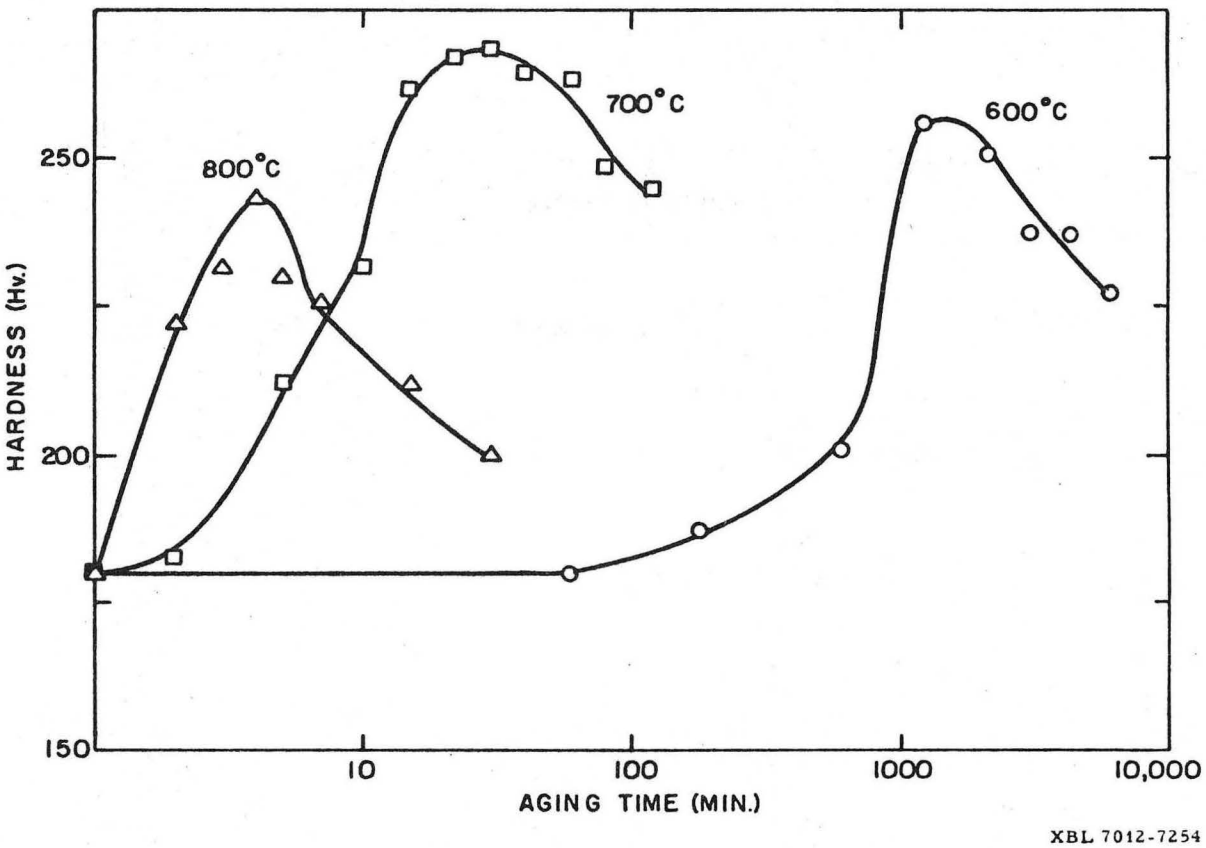
800°C
700°C
600°C
250
200
150
HARDNESS (Hv.)
10
100
1000
10,000
AGING TIME (MIN.)
XBL 7012-7254

Figure 35

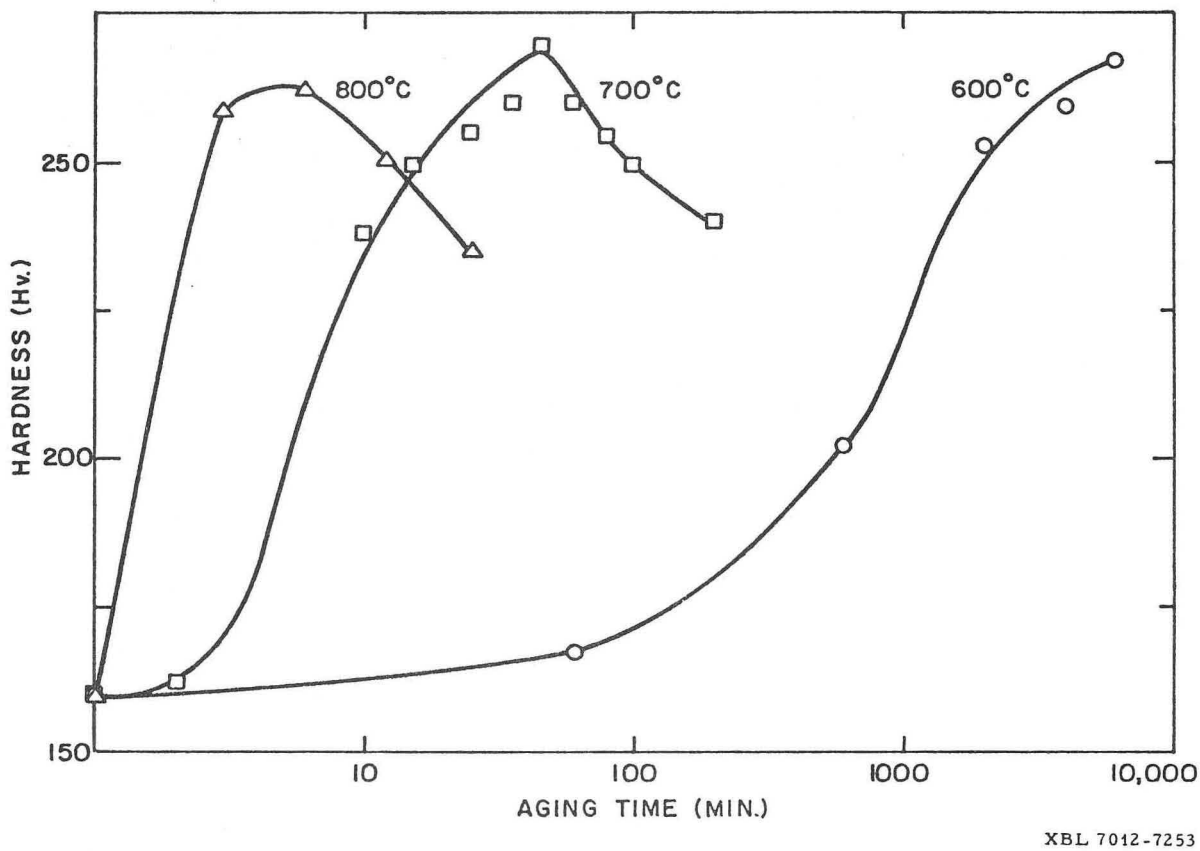
800°C
700°C
600°C
250
200
150
HARDNESS (Hv.)
10
100
1000
10,000
AGING TIME (MIN.)
XBL 7012-7253

Figure 36

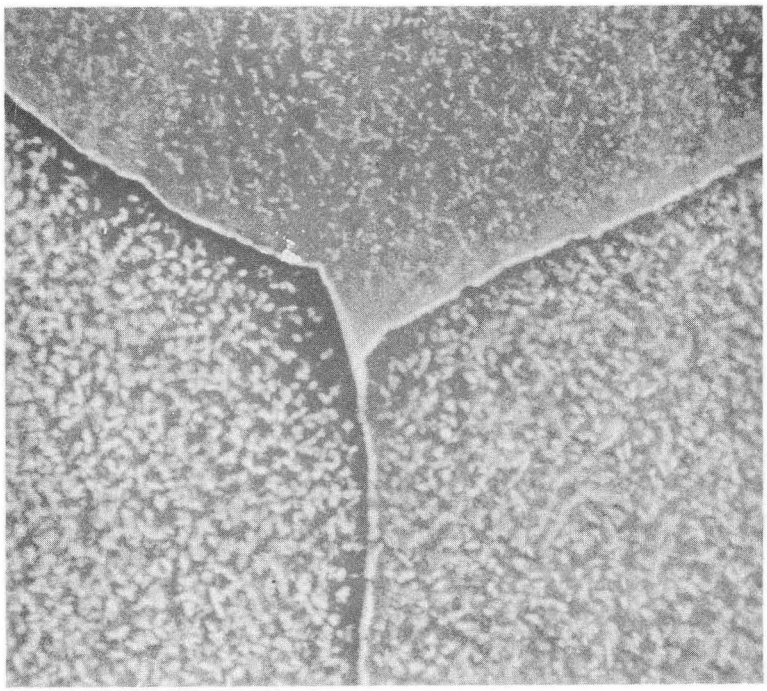

(a)

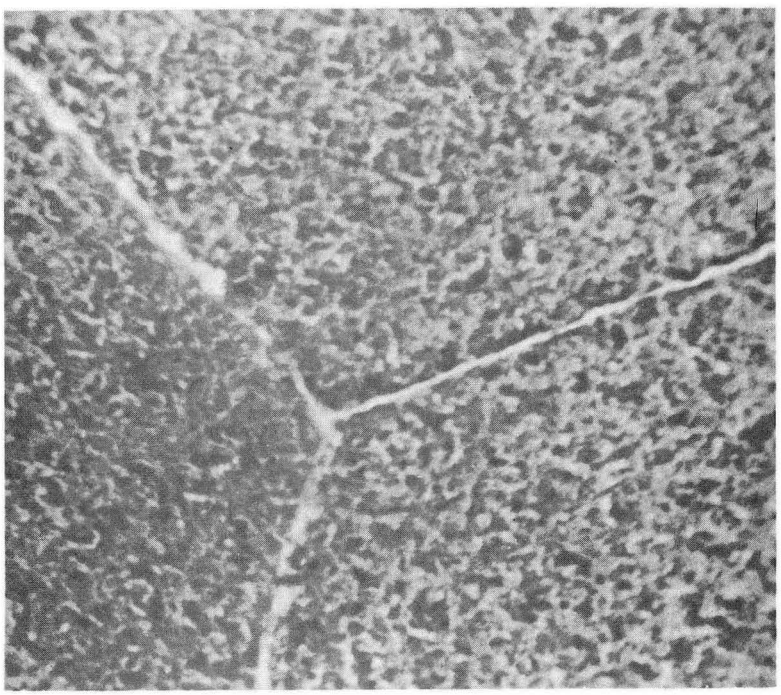

(b) XBB7012-5429

Figure 37

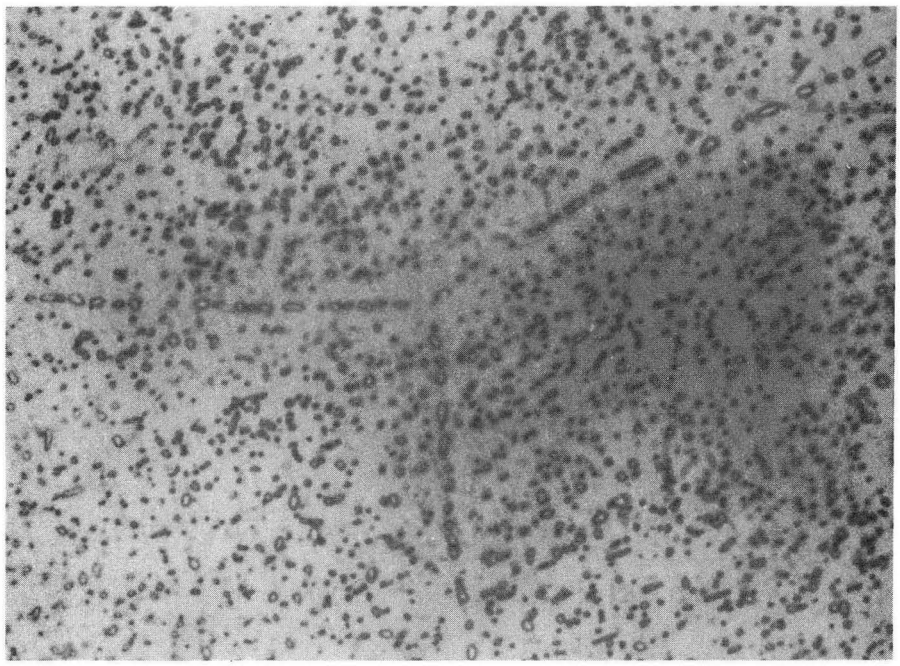

(a)

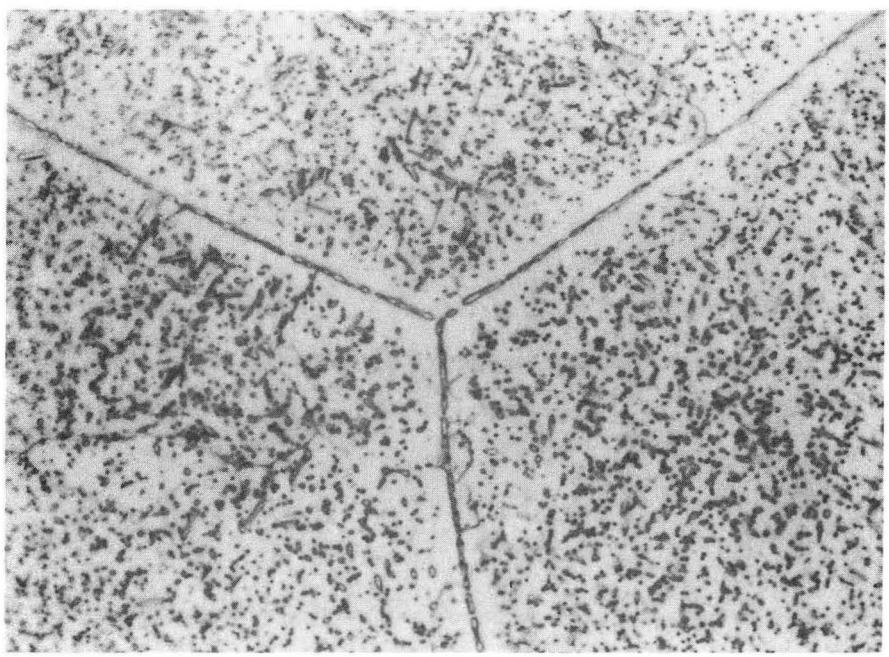

(b) XBB7012-5418

Figure 38

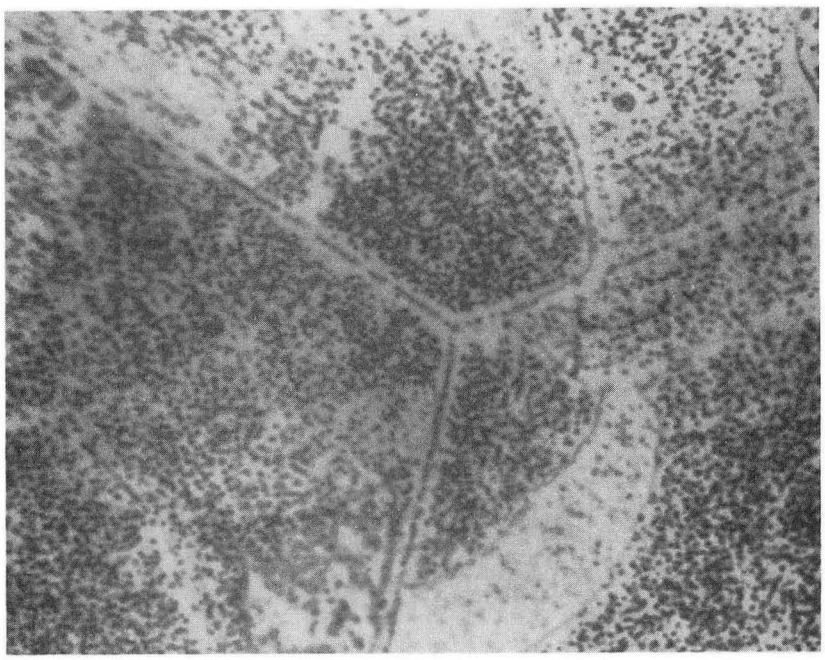

(a)

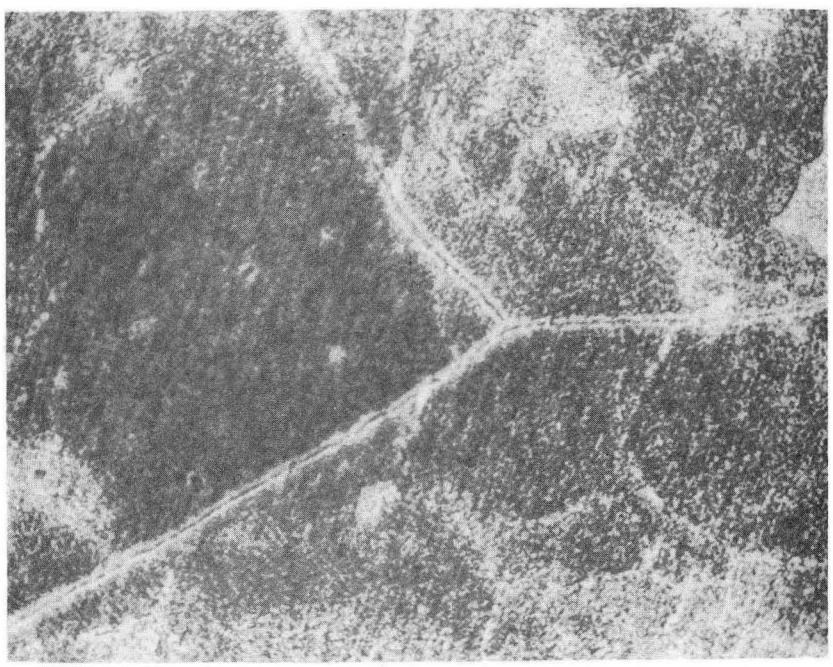

(b) XBB7012-5416

Figure 39

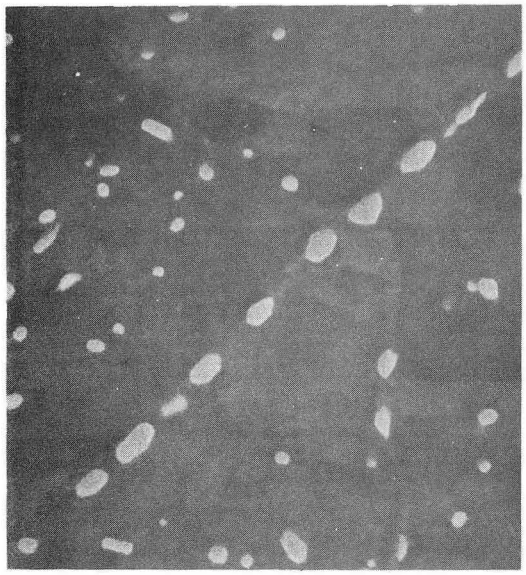

(a)

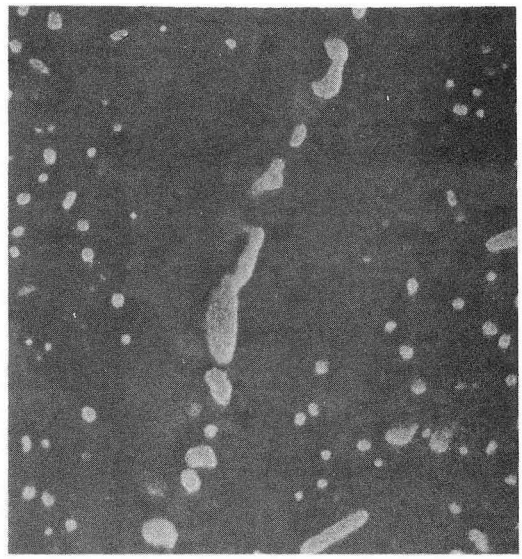

(b)

(c)

XBB7012-5412

Figure 40

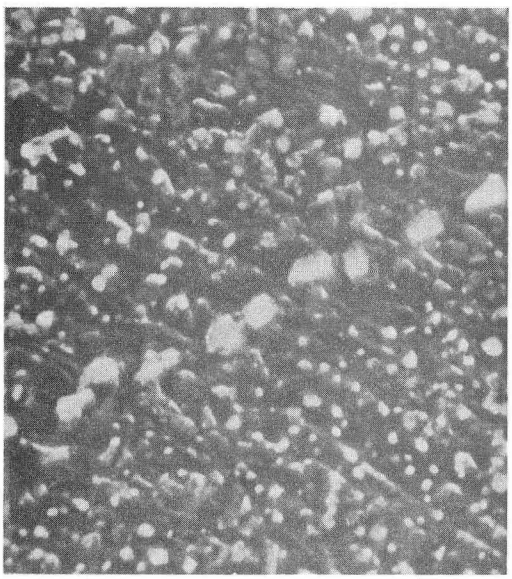

(a)

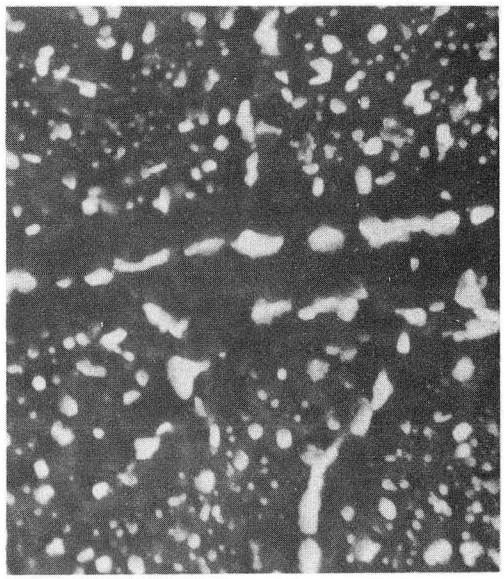

(b)

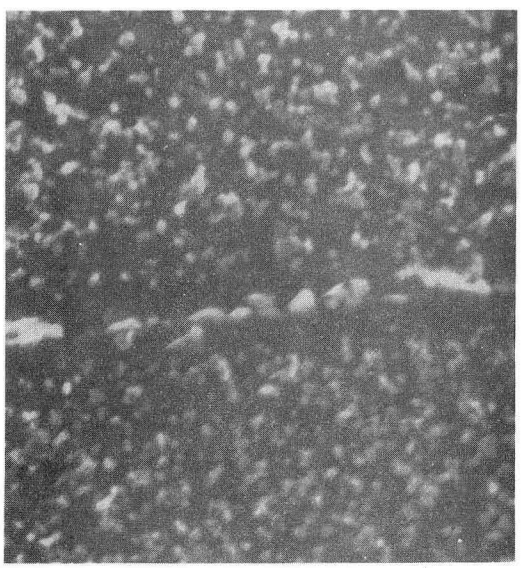

(c) XBB7012-5411

Figure 41

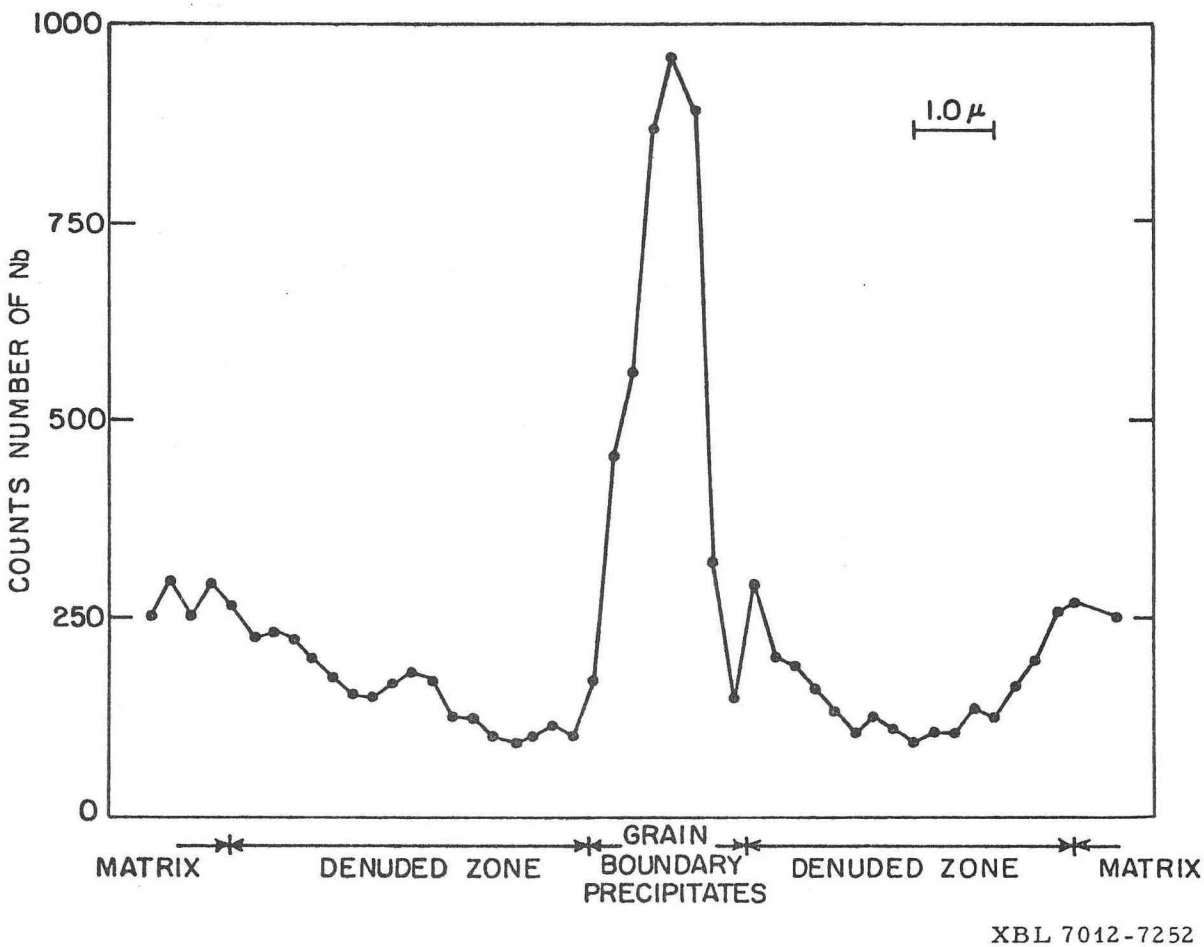
1000
750
500
250
0
COUNTS NUMBER OF Nb
1.0 μ
MATRIX
DENUDED ZONE
GRAIN BOUNDARY PRECIPITATES
DENUDED ZONE
MATRIX
XBL 7012-7252

Figure 42

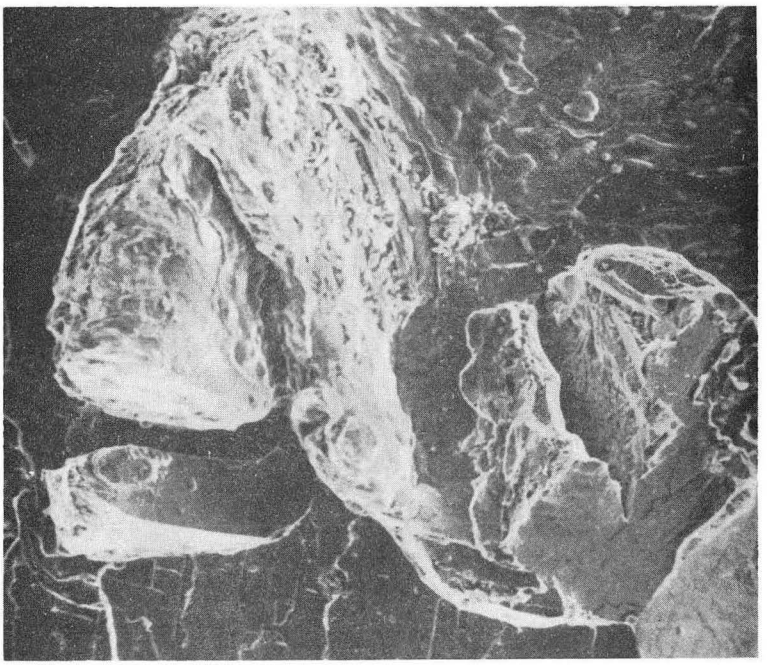

(a)

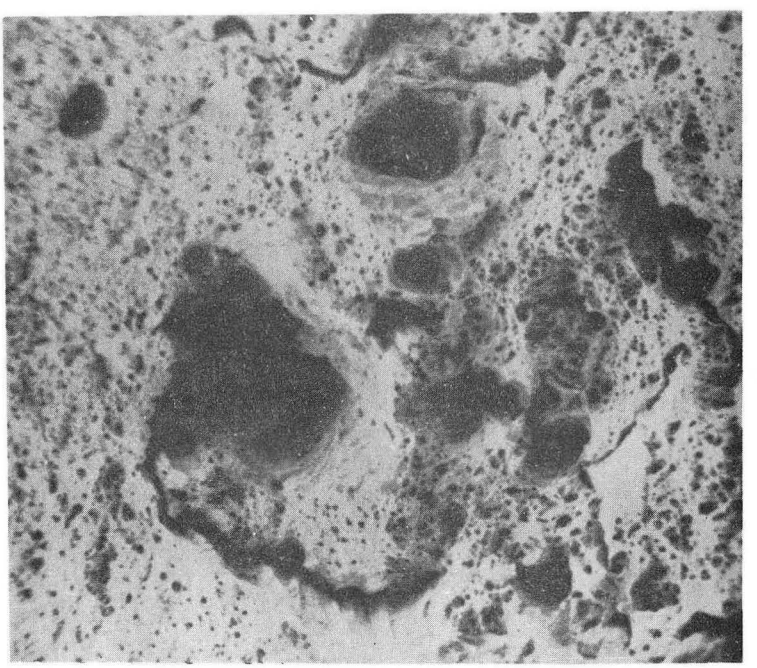

(b) XBB7012-5493

Figure 43

TECHNICAL INFORMATION DIVISION
LAWRENCE RADIATION LABORATORY
UNIVERSITY OF CALIFORNIA
BERKELEY, CALIFORNIA 94720